Remote Sensing of Environment 295 (2023) 113680

Contents lists available at ScienceDirect

Remote Sensing of Environment

journal homepage: www.elsevier.com/locate/rse

Grassland mowing event detection using combined optical, SAR, and weather time series

Ann-Kathrin Holtgrave [a,c,*], Felix Lobert [b,d], Stefan Erasmi [b], Norbert Röder [a], Birgit Kleinschmit [c]

[a] Thuenen Institute of Rural Studies, Bundesallee 64, Brunswick, 38116, Germany
[b] Thuenen Institute of Farm Economics, Bundesallee 63, Brunswick, 38116, Germany
[c] Geoinformation in Environmental Planning Lab - Technische Universitaet Berlin, Straße des 17. Juni 145, Berlin, 10623, Germany
[d] Earth Observation Lab - Geography Department - Humboldt-Universitaet zu Berlin, Unter den Linden 6, Berlin, 10099, Germany

ARTICLE INFO

Edited by Marie Weiss

Keywords:
Sentinel-1
Sentinel-2
Landsat 8
SVM
Random forest
CNN
LSTM
Backscatter
Interferomic coherence
CAP

ABSTRACT

The European Union's Common Agricultural Policy (CAP) and the Habitats Directive aim to improve biodiversity in agricultural landscapes. Both policies require enormous monitoring, which can be facilitated by remote sensing. Use intensity, measured by mowing frequency is an important indicator of biodiversity in permanent grasslands. The frequency and timing of mowing can be determined using satellite remote sensing because photosynthetically active biomass changes rapidly in response to mowing. However, the rapid regrowth of grasses requires very dense satellite time series for reliable detection. Radar time series can complement optical time series and fill in cloud-related gaps to overcome this problem. Additional weather data can support the detection of grassland mowing events, as mowing events are associated with specific meteorological conditions. However, previous studies have not fully exploited both potentials or different machine learning approaches for mowing event detection.

This study presents a new transferable two-step approach to detect grassland mowing events using combined optical and SAR data and additional weather data. First, we filled cloud-related gaps in optical time series using a supervised machine learning regression with optical and SAR data. We then classified time series sequences of optical, SAR and weather data into *mown* and *unmown* using four different machine learning algorithms. We used time series of NDVI and EVI (combined Sentinel-2 and Landsat 8), SAR backscatter, six-day interferometric coherence, backscatter radar vegetation index, backscatter cross-ratio (Sentinel-1), and temperature and precipitation sums. Our test sites are distributed across Germany and cover the entire gradient of grassland use intensities.

Mowing events could be detected with F1 values of up to 89%, first cut with up to 94%. Our results show no structural advantage of infilling time series with machine learning over linearly interpolated time series. The combined Sentinel-2 and Landsat-8 time series provided dense time series with mostly median gaps less than 20 days, which proved sufficient to reliably detect mowing events. SAR data were not essential for mowing event detection in our study, but weather data improved classification results for models trained on all areas and years. However, when the model was transferred to unknown years or areas that were not used for training, SAR data improved detection accuracy, whereas weather data degrade it. Models trained on all years but not all study sites detected mowing events with an accuracy of up to F1 = 76%. Models trained with all regions but not all years detected mowing events in untrained years with F1 up to 80%.

1. Introduction

Permanent grasslands make up about 19% of the land surface in the European Union (EU) and 14% in Germany (Eurostat, 2018; Statistisches Bundesamt, 2019). They play a crucial role in nature conservation by promoting the diversity of vegetation, insects, and birds (Klimek et al., 2007; Kleijn et al., 2009; Wrage et al., 2011; Socher et al., 2012; García-Feced et al., 2015). In Germany, more than half of all animal and plant species can be found in grasslands. Grasslands help to prevent flooding, as they have a high water storage capacity and good infiltration properties (Mitsch and Gosselink, 2000; Fischer et al., 2015). By reducing the input of nutrients and pollutants into water bodies, it contributes to water quality (Jankowska-Huflejt,

* Corresponding author at: Thuenen Institute of Rural Studies, Bundesallee 64, Brunswick, 38116, Germany.
E-mail address: a.holtgrave@tu-berlin.de (A.-K. Holtgrave).

https://doi.org/10.1016/j.rse.2023.113680
Received 15 June 2022; Received in revised form 2 June 2023; Accepted 5 June 2023
Available online 24 June 2023

2006). Moreover, intact grasslands have a positive impact on climate change by storing greenhouse gases such as carbon dioxide and nitrous oxides (Soussana et al., 2004). In addition, they contribute to the aesthetics of the landscape and are an important cultural heritage. Permanent grasslands are also an important source of feed for livestock for milk and meat production, as well as a source of biomass for energy production (Ketzer et al., 2017; Peeters, 2009). However, there is often a trade-off between environmental and economic value of grasslands. High biodiversity requires low use intensity, while high use intensity is associated with high profitability.

To address the loss in biodiversity in Europe, the EU has implemented several policy instruments. To promote sustainable agriculture and thus biodiversity in particular, the EU's Common Agricultural Policy (CAP) provides instruments to compensate farmers through subsidies for losses due to environmentally sound management in low-input systems (European Union, 2021a). National CAP paying agencies are responsible for monitoring and evaluating the effectiveness and implementation of the CAP measures. The EU Habitats Directive (Council Directive 92/43/EEC) requires national governments to designate areas for the conservation of animal and plant species. The designated sites must be monitored, their conservation status must be reviewed, and measures must be developed to improve or maintain a favorable conservation status in order to fulfill the obligations of the Habitats Directive to restore, maintain, and promote biodiversity. In the future, remote sensing technology will reinforce CAP controls (European Commission, 2018; European Union, 2021b) and can support the obligations of the Habitats Directive by replacing and complementing costly physical on-site inspections or site assessments (Corbane et al., 2015).

One of the standard CAP measures for grassland areas is the prohibition of mowing before a certain date (e.g. Richtlinie NiB-AUM, 2019; Richtlinie KULAP, 2020). Early mowing can reduce biodiversity by preventing flowering plants from completing their reproductive cycle and disturbing ground-nesting birds (Smith et al., 2000; Brown and Nocera, 2017). The number and frequency of mowing events per year also influence which plants can regenerate, with high frequencies allowing only a few grassland species to establish, resulting in low biodiversity (Schoof et al., 2020). However, mowing later for biodiversity can mean a reduction in yield or forage quality and mowing less times than possible a reduced monetary value (Brown and Nocera, 2017). Therefore, it is possible to infer the use intensity from the number of mowing events or the intervals between them (Döhler, 2009; Weiner et al., 2011). Also, the date of the first cut is an indicator of the intensity of use, as an early first cut indicates a highly productive grassland that is managed intensively. Thus, the detection of mowing events by remote sensing can help to control CAP measures and identify grassland use intensities to inform decision makers. It can support the monitoring of the Habitats Directive and other policies and monitoring programs at the interface between agriculture and nature conservation.

To determine the intensity of grassland use from detected mowing events, there are three ways to consider: the number of mowings per parcel and year, the month of the first mowing date, or the period between mowings (see Table 1). All three indicators are related to the amount of time the grass grows before being mowed. At a certain state of growth, the quality of fodder decreases with increasing biomass (McIntosh et al., 2016; Waramit et al., 2012). In intensively managed grasslands, where forage value is often a priority, fast-growing grassland species with low species diversity are used and given less time to grow to produce the highest possible forage quality. As a result, the first cut is made early in the year, the grass has little time to regenerate and is cut more frequently throughout the year. In extensive grassland, the benefits of forage are often secondary. In some cases, management is more about minimum use or ecological motives, as more extensive grassland has higher biodiversity. The first mowing starts later, often because of environmental regulations. Where extensive grassland is mown more than once a year, there are long periods between mowings.

Table 1
Apportionment of intensity levels of grassland usage in agriculture in Germany.
Source: Adapted and abridged according to Rieder (1997) and Dierschke et al. (2002).

Criteria	Intensity level		
	Extensive	Medium	Intensive
No. of mowings [n]	1–2	3–4	5–6
Recovery period [d]	>75	40–75	<40
First Usage [month]	June or later	May	April

A growing number of remote sensing studies are investigating the detection of mowing events, as the abrupt change in biomass and vegetation height causes significant changes in spectral reflectance behavior and surface roughness. For a detailed review of remote sensing studies of grassland production and management see Reinermann et al. (2020). Optical vegetation indices (VIs), derived from remote sensing satellites such as Sentinel-2 (S2) or Landsat, have demonstrated their ability to detect mowing events based on the spectral reflectance properties of optical data (Courault et al., 2010; Halabuk et al., 2015; Estel et al., 2018; Kolecka et al., 2018; Griffiths et al., 2019; Schwieder et al., 2022; Reinermann et al., 2022). The most commonly used VIs in these studies are the Normalized Difference Vegetation Index (NDVI) (Rouse et al., 1973) and the Enhanced Vegetation Index (EVI) (Huete et al., 2002). Although optical data is valuable for this task, cloud-caused gaps in the optical time series can be a problem. Grass can regrow fast after a cut. Therefore, the detection of mowing events is time-critical and gaps in time-series can lead to missed events and wrong use intensity estimations. Many attempts have been made to fill the gaps in time series with mono-sensor data using past and future data for interpolation at different levels of complexity from linear interpolation to deep learning methods (Chen et al., 2019; Julien and Sobrino, 2019; Kandasamy et al., 2013; Jin et al., 2021; Belda et al., 2020). Some studies harmonized different optical sensors to fill the gaps (Moreno-Martínez et al., 2020; Claverie et al., 2018; Bolton et al., 2020; Frantz, 2019). However, the application of Gap-handling approaches other than interpolation for mowing event detection is rare.

Radiation in the microwave domain provides weather-independent, almost seamless time series, but radar data from e.g. Sentinel-1 (S1) Synthetic Aperture Radar (SAR) are more complex to interpret than optical data. Nevertheless, SAR can be used to detect mowing of grassland. The signal reflected from the ground represents the surface conditions and is influenced by vegetation structure, biomass, and height, among other factors. Backscatter is the portion of the outgoing radar signal that is reflected directly back to the radar antenna by the target. Combining two SAR images taken at different times produces interferometric images. Changes between the two scenes cause a loss of interferomic coherence, which can be used to detect modifications (Rosen et al., 2000). Removing grass by mowing changes the height and biomass of vegetation abruptly, causing alterations in both backscatter and coherence of the SAR signal. These alterations have more significant effects on coherence (Lobert et al., 2021; de Vroey et al., 2021). Successful detection of mowing events using backscatter alone has been reported by Schuster et al. (2011), Grant et al. (2015a), and Siegmund et al. (2016). Taravat et al. (2019) calculated additional grey-level co-occurrence (GLCM) second-order texture metrics from S1 backscatter, resulting in an overall accuracy of 85.7%. While Zalite et al. (2014, 2016) used coherence and partially backscatter for mowing event detection on a small sample size of eleven sampling plots and eight COSMO-SkyMed scenes, de Vroey et al. (2021) employed S1 backscatter and coherence data on a region-wide dataset with coherence having the higher explanatory power. Quad-polarimetric SAR has not been widely used due to the limited availability of suitable satellites, and it has not been as successful as the other approaches (Voormansik et al., 2013).

Weather data can provide additional information and support satellite imagery in detecting mowing events. Rainfall and temperature

have a significant impact on vegetation condition and satellite signal. Rainfall and temperature affect grass productivity and the rate at which grass regrows after a cut (Smit et al., 2008). Additionally, farmers rarely mow on rainy days. The date when grass starts to grow after winter is the sustainable start of grassland vegetation. This date can be predicted roughly by the weighted sum of average daily temperatures from January onwards (grassland temperature sum). This is also known as the beginning of the agro-meteorological spring (Ernst and Loeper; Bundesanstalt für Landwirtschaft und Ernährung, 2017). Remote sensing data prior to this date is mostly influenced by environmental factors such as rain and soil moisture, or by management activities other than mowing such as fertilizer spreading or rolling. Therefore, remote sensing data before the start of the growing season can introduce problematic patterns in algorithm training and misinterpretations in application.

Weather data, especially when working with SAR data, can support the detection of mowing events in remote sensing models (Garioud et al., 2020; Zalite et al., 2016; Buddeberg et al., 2016). This is because meteorological conditions affect the water content of plants, and therefore the satellite signal. Soil moisture, which is influenced by precipitation and temperature, also has a significant direct effect on the SAR signal (Li et al., 2021). Precipitation on the same day as the SAR acquisition can distort the signal due to interception.

Although both optical and SAR data have been shown to be valuable for mowing event detection, only a few studies have used both together, and even fewer have used additional weather data. For instance, Stendardi et al. (2019) compared S1 backscatter coefficient and S2 NDVI for mowing event detection. Their analysis suggested possible synergies, but they did not propose a method for joint use. Sen4CAP (esa.sen4cap.org) already includes a tool for detecting mowing events on grassland using S1 coherence and S2 NDVI. de Vroey et al. (2021) evaluated the algorithm against a reference dataset in Belgium and found that 79% of mowing events were detected. However, with only 58% true positives and 42% false positives, the accuracy is relatively low. In a hierarchical approach, de Vroey et al. (2023) first differentiated grassland into grazed pastures and mown hay meadows. They then used the Sen4CAP toolbox to detect mowing events on hay meadows only with an accuracy of 93% and a detection rate of 82%. Lobert et al. (2021) combined S1 backscatter and GLCM, six-day coherence, as well as S2 and Landsat 8 (L8) NDVI data and performed a grid search for the best combination of features to detect mowing events. Their results showed only a slight improvement of the combined use compared to the separate use of SAR or optical data, with the optical data having a significantly higher explanatory power. Reinermann et al. (2022) combined time series of optical EVI data (S2) with InSAR, PolSAR, and backscatter features (S1) for a rule set approach. Again, the optical data proved to be the most informative for mowing event detection. PolSAR data were able to provide support, especially for longer cloud induced gaps in the EVI time series but also introduced more false-positive detections. Again with S1 coherence and S2 NDVI de Vroey et al. (2022) was able to detect mowing events with an F1-score of 79% on hay meadows.

Combined optical and SAR features have shown their potential for mowing event detection. However, the potential is not fully exploited. The joint use of optical and SAR data also provides an opportunity to fill cloud-induced gaps in the optical time series, thereby creating an artificial optical time series and reducing the risk of undetected events. Many recent studies have attempted to synthetically fill optical data gaps with optical and SAR data using machine learning (ML) techniques (e.g. Mazza et al., 2018; Scarpa et al., 2018; Schmitt et al., 2018; Bermudez et al., 2019; Cresson et al., 2019; Wang et al., 2019b). These attempts focused primarily on the spatial filling of clouds in one satellite scene, but sometimes also included temporal information (Zhao et al., 2020). Although some of these studies have been very successful in filling cloudy pixels with artificial values, the methods are often quite complex and, being raster-based, are computationally and memory intensive in training and application. Object-based approaches have also been investigated. Holtgrave et al. (2020b) compared S1 and S2 data over agricultural areas to test whether they behave in the same way over the course of the year and therefore whether S1 data can replace S2 data in the case of cloudy S2 scenes. Garioud et al. (2020, 2021) successfully used a Recurrent Neural Network (RNN) with optical and SAR data, weather, and topography information to infill optical time series for grassland, crop and forest monitoring. However, to fill in the gaps, the approach requires data from the whole year. Therefore, statements about mowing could only be made at the end of the year. Such a late analysis would be too late for CAP controls. In case of doubt about the results of a mowing detection, on-site controls would still have to be carried out. It is therefore important that the analyses are carried out as soon as possible. Wang et al. (2019a) employed Random Forest and Support Vector Machines (SVM) to predict Leaf Area Index (LAI) time series at two sites with joint optical and SAR data. Unlike most studies, the models were tested for transferability to other years. The combined data overcame the disadvantages of the individual sensors: SAR can be affected by soil at low biomass and optical data tend to saturate at high biomass.

Aside from gap filling, ML methods are also applied in many other remote sensing fields, including agriculture (Liakos et al., 2018). So far, Halabuk et al. (2015), Taravat et al. (2019) and Lobert et al. (2021) have used ML for mowing detection. The first used a Classification and Regression Trees (CART) algorithm, the second a Multilayer Perceptron (MLP) and the third a Convolutional Neural Network (CNN). The three studies classified small consecutive sequences of the grassland time series into *mown* and *unmown*. An advantage of machine learning approaches is that they do not require expert knowledge of grassland development. Patterns and correlations can be identified in large, multidimensional data sets without human intervention (Dahiya et al., 2022). Other studies rely on change detection by thresholding or rule sets for mowing event detection (Courault et al., 2010; Grant et al., 2015a; Estel et al., 2018; Kolecka et al., 2018; Griffiths et al., 2019; Stendardi et al., 2019; de Vroey et al., 2021; Schwieder et al., 2022; de Vroey et al., 2022).

Previous remote sensing studies did not fully exploit the combinations of different input features from optical, radar, and weather data in deep learning approaches to detect mowing events. Advances in data policy, making the Sentinel and Landsat satellite data freely available can and should now be fully exploited. Exploring the potential of different machine learning and deep learning methods has not been done for mowing event detection. Most studies to this point do not test their models for transferability to other sites and years but this would especially important to apply an approach area-wide and make it valuable for CAP or Habitat Directive monitoring. Therefore, the aim of this study was to develop a feasible approach to monitoring mowing events that allows spatial and temporal extrapolation to years and areas that were not included in the training data. The approach should also be continuously applicable throughout the whole growing season and not only at the end of the year. We used both optical and SAR remote sensing data in combination with weather data and a novel two-step approach to fill gaps in optical time series with supervised ML regression and then classified time series sequences into *mown* and *unmown* using ML methods. We compared four different ML algorithms and consider the usefulness of SAR, optical, and meteorological features. Our reference data came from various grassland sites in Germany, covering representative geographical regions over several years and representing all intensity levels from extensive to intensive. We also investigated the transferability of our approach in time and space.

This study aimed to answer the following questions:

(1) Can the detection of grassland mowing events be improved by gap filling in optical time series with SAR data using machine learning algorithms? (2) Can additional precipitation and temperature features improve the results? (3) Can we transfer the trained model to unknown years and regions?

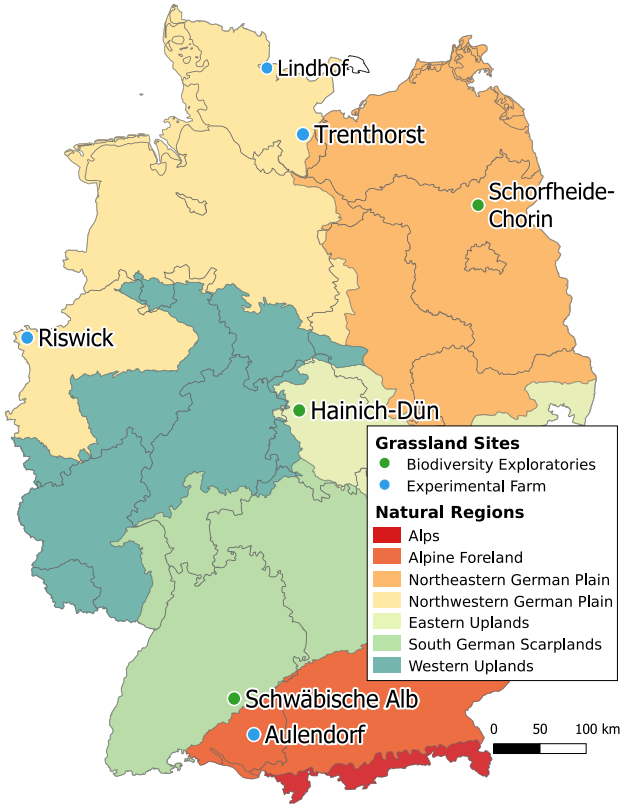

Fig. 1. Locations of Study sites across Germany.

2. Material

2.1. Study sites

The study was carried out at seven grassland sites in the Federal Republic of Germany. Germany has a temperate climate with an average temperature of 9.0 °C and an average precipitation of 721 mm (DWD Climate Data Center, 2021a,c). Grassland in Germany is mostly semi-natural permanent grassland in the form of meadows, pastures and hay meadows. It is managed for nature conservation or for fodder production.

The study sites are widely distributed throughout Germany and have different climatic and soil conditions. They cover five of the seven natural regions in Germany (see Fig. 1). Lindhof and Trenthorst have a maritime influence, Haus Riswick is situated in the warm lowlands, the Schwäbische Alb is a low mountain range with comparatively lower temperatures and well-drained soils, Aulendorf is in the warmer and wetter uplands, and Schorfheide-Chorin is again situated in the relatively dry lowlands. Hainich-Dün lies in a transition area between the low mountain range of eastern Hesse and arable plains.

2.2. Reference data

We used data from seven study sites representing the heterogeneity of the German grassland landscape in 2017, 2018 and 2019 (see Table 2). The different study sites represent a gradient of intensity, ranging from plots mown once or twice a year to more intensively managed areas with up to five cuts per year.

We collected the data from experimental farms of Federal Ministries of Agriculture, research institutes, or universities, which keep permanent records of their grassland parcels and management practices. Another source of ground truth data were three intensively studied grassland areas of the Biodiversity Exploratories (Fischer et al., 2010; Vogt et al., 2019). All seven study areas together provided information on 175 parcels in 2017, 190 parcels in 2018 and 133 parcels in 2019. A total of 1200 mowing events were recorded.

Table 2
Overview over study sites ordered from north to south with site name, available years, precipitation sum, average temperature, number of mowing events, and number of parcels per year. The number of parcels includes all parcels with at least one mowing and no grazing before the first mowing.

Study site	Year	Precipitation sum [mm]	Temp. avg [°C]	No. of cuts	Median no. of cuts	No. of parcels
Lindhof	2017	965	9.7	1–4	3	5
	2018	575	10.2	1–4	2	14
Trenthorst	2017	913	9.7	1–2	1	6
	2018	507	10.5	1	1	8
	2019	711	10.5	1–2	2	11
Schorfheide	2017	736	9.8	1–2	2	18
Chorin	2018	418	10.8	1–2	1	22
	2019	520	11.0	1–2	1	15
Riswick	2017	777	11.3	3–4	3	27
	2018	669	12.2	1–4	4	27
	2019	797	11.9	4	4	19
Hainich	2017	891	9.2	1–2	1	23
	2018	540	10.1	1–2	1	21
	2019	698	9.9	1–2	1	25
Schwäbische	2017	1147	8.2	1–4	2	43
Alb	2018	887	9.1	1–4	2	46
	2019	1102	8.6	1–4	2	45
Aulendorf	2017	1156	9.0	1–5	3	53
	2018	888	9.9	1–5	4	52
	2019	1088	9.4	5	5	18

All datasets for all study sites consisted of parcel boundaries and information on grassland management practices and the corresponding date or day of the year. The minimum management information included grassland harvest dates. Data did not always include information on grazing. In this case, we treated the parcels as grassland with no grazing activities. We focused on parcels with at least one mowing. We did not include pure pasture plots because we did not have information on pasture management, such as livestock density or rotation, for all study sites. In the case of hayfields with both mowing and grazing information, we included data from the beginning of the year in the training dataset until the first grazing occurred.

2.3. Satellite data

The SAR satellite constellation with two Sentinel-1 (S1) satellites S1-A and S1-B and the optical satellite constellation with two Sentinel-2 (S2) satellites S2-A and S2-B and Landsat 8 (L8) acquired the images used in this study. We used available S2 and L8 data for all test sites for the respective years, but where S2 and L8 acquired data on the same day, we kept only the S2 scene due to its higher spatial resolution. For the S1 data, we selected one orbit for each test site to ensure consistent acquisition geometries for all images. To avoid signal interference from morning dew, we only selected ascending orbits acquired at around 5 pm (Tamm et al., 2016). Fig. 2 shows the availability of the satellite data for the study years and study sites.

S1 operates in C-band (5.5 cm wavelength) and mainly provides dual-polarization data in VV (vertical transmit, vertical receive) and VH (vertical transmit, horizontal receive) in the interferometric wide swath (IW) mode. The S1 constellation has a revisit time of 6 days on the same orbit (Hajduch and Bourbigot, 2022).

Repeatpass SAR coherence is a measure of the decorrelation between two co-registered images (Rosen et al., 2000). Changes between two SAR images cause a decrease in interferomic coherence. We generated coherence time series from S1 single look complex (SLC) products, which contain phase and amplitude information. The coherence between each image and the image acquired six days earlier was calculated for VV and VH polarization, respectively. This was done by updating all orbit positions and co-registering the corresponding

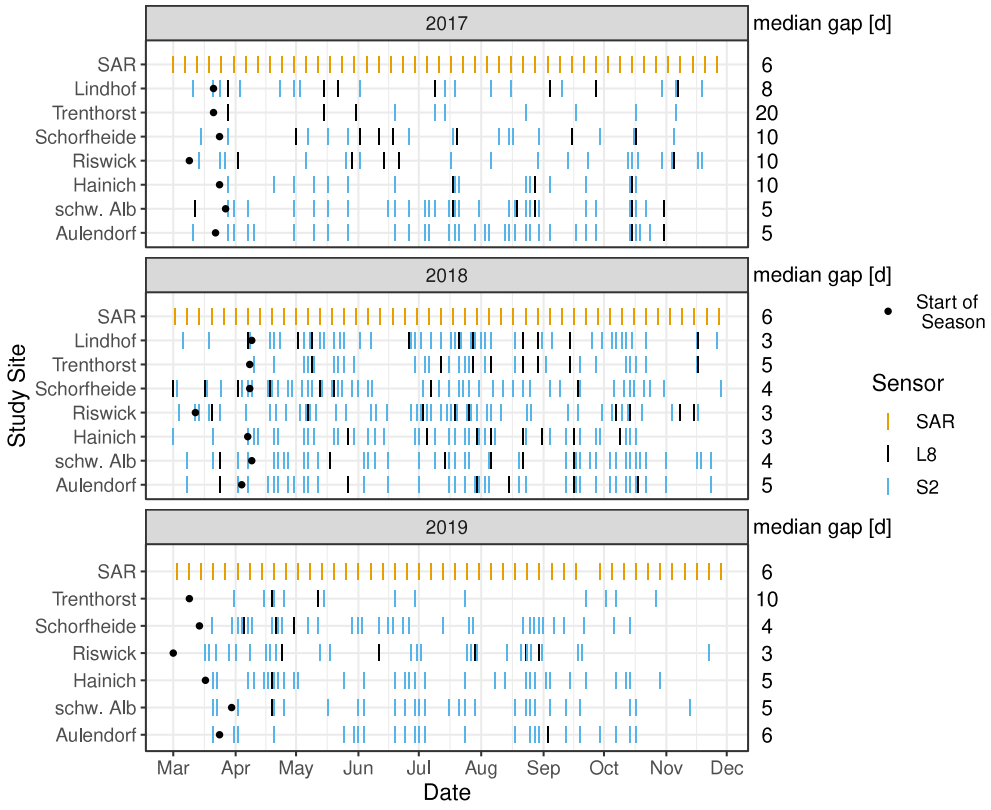

Fig. 2. Availability of cloud free optical data from Sentinel-2 (S2) and Landsat 8 (L8) for the study sites and the availability of one Sentinel-1 (S1) orbit with its six-day revisit interval. The sustainable start of growing season and the median number of days between two acquisitions per year are shown.

image pairs using SNAP-ESA Sentinel Application Platform software. The coherence images were then debursted and terrain corrected. A total of 1289 individual scenes were processed in this way.

We processed 1617 backscatter images from Ground Range Detected (GRD) products that were detected, multi-looked, and projected to the ground range with phase information lost. On the GRD data, we performed the standard pre-processing steps thermal and border noise removal, calibration, and terrain correction to calculate the gamma-naught backscatter coefficient in VH and VV polarization for each image with SNAP (Filipponi, 2019). A speckle filter was not necessary because we used an object-based approach. After preprocessing, the backscatter and coherence images had a resolution of 10 x 10 m. From S1 VV and VH backscatter, the Radar Vegetation Index (RVI)

$$RVI = \frac{4 \cdot VH}{VH + VV} \tag{1}$$

and the VH/VV ratio were calculated. They showed their potential for agricultural vegetation monitoring as they are more robust against environmental impacts (Holtgrave et al., 2020b; Schlund and Erasmi, 2020; Nasirzadehdizaji et al., 2019; Vreugdenhil et al., 2018).

S2 has 13 optical bands with wavelengths between 443 and 2202 nm and spatial resolutions of 10, 20, or 60 m. S2 has a revisit time of 10 days at the same viewing angles (Thales Alenia Space Team, 2022). L8 acquires images in 9 bands from 430 to 1380 nm with a revisit time of six-days. Except for the panchromatic band, L8 images have a spatial resolution of 30 m (United States Geological Survey, 2019). For optical imagery, the viewing angles are neglected in this study. The overlap of the different orbits at higher latitudes, therefore, allows for a higher revisit frequency. Fig. 2 shows the availability of S2 and L8 scenes for the different sites.

Analysis-ready data (level-2) were provided by a FORCE data cube. The S2 and L8 scenes were radiometrically and geometrically corrected, reprojected and cloud masked using the FORCE (Framework for Operational Radiometric Correction for Environmental monitoring) processing system (Frantz, 2019). During this process, the L8 resolution was adjusted from 30 m to 10 m using nearest-neighbor resampling. The VIs NDVI (Rouse et al., 1973) and EVI (Huete et al., 2002) were then calculated using the FORCE processor. In grassland studies, the joint use of NDVI and EVI can be an advantageous, because they respond in complementary way (Halabuk et al., 2015).

We calculated the pixel median of each grassland parcel for each optical and SAR scene feature after applying an inward buffer of 12 m to the parcels to avoid mixed pixels at parcel boundaries.

2.4. Weather data

The three years considered, 2017–2019, had different weather conditions. 2017 was a wet year, while 2018 was extremely dry, warm and with above average sunshine hours (DWD Climate Data Center, 2021a,c,b). 2019 was also warmer and drier than average, but not as extreme as 2018.

We used daily weather data from the German Weather Service (DWD) in a one-kilometre grid (German Weather Center, 2020). We averaged the mean temperature in ° C and the precipitation sums in mm for each study site and day and calculated three, six, and 12-day right aligned rolling sums. By using rolling precipitation and temperature sums, the weather of previous days is considered to reflect the growing conditions for the plants or the management conditions.

We calculated the *corrected cumulative grassland temperature sum* for each study site and year to obtain the day of the *sustainable vegetation start* (Ernst and Loeper; Bundesanstalt für Landwirtschaft und Ernährung, 2017). For the corrected cumulative sum, all positive daily temperature averages from the beginning of the year are added. In January temperatures are multiplied by a factor of 0.5, in February by a factor of 0.75, and thereafter by a factor of 1. If the cumulative sum exceeds 200 in spring, the sustainable start of vegetation has been reached. The date is used to exclude satellite scenes from our dataset

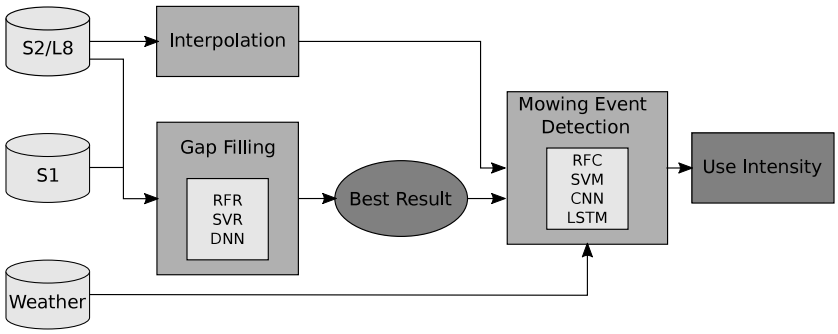

Fig. 3. Schematic depiction of method. Different machine learning and deep learning methods were tested (RFR: Random Forest Regression, SVR: Support Vector Regression, DNN: Deep Neural Network, RFC: Random Forest Classification, SVM: Support Vector Machine, CNN: Convolutional Neural Network, LSTM: Long Short-Term Memory).

Table 3
Overview of input data for gap filling and for mowing event detection.

Type	Feature	Gap Filling	Mowing event detection					
			OPT+SAR		OPT		SAR	
			+W	−W	+W	−W	+W	−W
SAR	Backscatter	x	x	x			x	x
(VV, VH)	Coherence	x	x	x			x	x
	RVI, Ratio	x	x	x			x	x
Optical	NDVI	x	x	x	x	x		
	EVI	x	x	x	x	x		
Weather	Temperature		x		x		x	
	Precipitation		x		x		x	

prior to the sustainable vegetation start individually for each study site and year. The temperature differences between the years and between the different study sites lead to different starts of the growing season (see Fig. 2).

2.5. Features

After processing the satellite scenes, we had different SAR, optical, and weather features in time series for each parcel. In the following, these features were used for gap filling and time series classification. To fill the gaps, we also used the information from the period between successive optical scenes. As we also wanted to determine the importance of optical, SAR and weather features we compared different feature groupings: Optical and SAR features together (OPT+SAR), optical features only (OPT), and SAR features only (SAR). We compared each group with weather data (+W) or without weather data (−W). Table 3 shows an overview of all different features and in which method and grouping they are deployed.

3. Methods

Mowing event detection is time-critical because grass can grow back very quickly after a mowing event, which could easily result in an event being missed if satellite imagery is not available. Due to cloud cover, optical data time series can have long gaps between scenes. Therefore, in a first step, we wanted to fill the gaps in optical time series with different machine learning regression methods. In a second step, we use ML techniques to classify time series snippets into *mown* and *unmown* (see Fig. 3).

3.1. Gap handling

All data must be on the same temporal grid for SAR, optical, and weather data to be used together in a binary classification of time series snippets, as not all ML algorithms used in this study can work with missing values. We used the S1 data in its regular six-day interval as the reference grid. We fitted temperature and precipitation data to this grid using only weather data from the same days as the S1 data. The availability of optical data from S2 and L8 does not have a regular time interval due to clouds and different sensing geometries. The aim of the gap filling was therefore to produce artificial optical data on the days of the S1 acquisitions when no actual optical data were available to match with the temporal grid.

A simple approach to fill gaps in time series is linear or spline interpolation between existing data (e.g. de Carvalho et al., 2017). However, this can lead to over- or under-estimation of actual values, resulting in mowing events going undetected. We therefore tested three machine learning algorithms in addition to a linear interpolation to fill the optical time series grid with the help of SAR data based on our previous findings (Holtgrave et al., 2020a,b).

To train and test the Gap-handling approaches, we created a dataset of days with both SAR and optical data available. The presence of such coincident data was assessed individually for each grassland parcel. For all parcels combined, this resulted in 5245 samples across all years. The two previous (t_{-1}, t_{-2}) and two subsequent (t_1, t_2) optical and SAR data were assigned to each of these samples at the time of t_0, regardless of whether they were on the six-day grid (see Fig. 4). For the SAR data, the six-day repeat time resulted in a window size of five observations and 24 days. For the optical data, the window size is also five observations, but the number of days within the window varies depending on cloud conditions. Therefore, the days between optical observations were also added as a feature. The target variable of this regression task was the vegetation indices at t_0 and the input variables were all other features at t_{-1}, t_{-2}, t_1 and t_2. In addition, the SAR features at t_0 were included in the regression task. 80% of the samples were used as training data and 20% as test data, including all parcels and years. In the test dataset, the optical target variable was removed at t_0 to create synthetic gaps.

We tested Random Forest Regression (RFR), Support Vector Regression (SVR), and a Deep Neural Network Regression (DNN) to generate artificial optical data at data gaps. Random forest is a classification and regression method that consists of multiple uncorrelated decision trees. All decision trees are grown under a particular type of randomization during the learning process (Ho, 1995; Breiman, 2001). In regression tasks, the average prediction of the individual trees is returned. Random Forest is a widely used method for remote sensing applications due to the accuracy of the results and the direct evaluability of the variable importance (Belgiu and Drăgu, 2016). We used the *ranger* method from the R package *caret* with 10 k-fold cross validation (Kuhn et al., 2021). SVR is based on Support Vector Machines (SVM) for classification purposes developed by Vapnik (2000). In SVR, the original non-linear function is transferred to a higher dimensional feature space where the function can be treated as a linear function. Linear regression can be applied, and an optimal approximation can be obtained. SVMs were introduced years before Random Forest, but are still of great interest in the remote sensing community (Mountrakis et al., 2011; Sheykhmousa et al., 2020). From *caret* we employed the *svmRadial* method with 10 k-fold cross validation. Both RF and SVR use an automatic grid

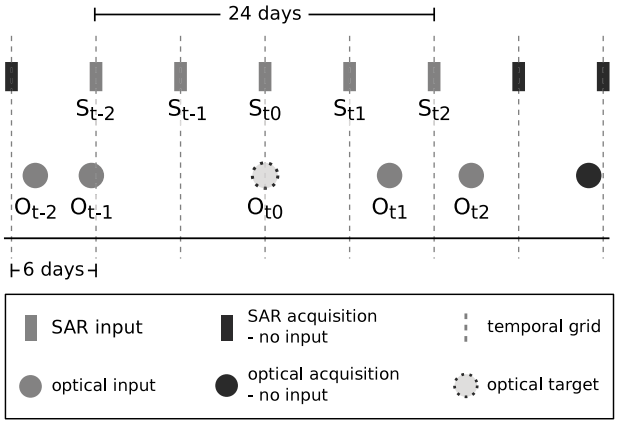

Fig. 4. Schematic depiction of gap filling. The target variable are the vegetation indices at t_0 and the input variables are the optical and SAR features at t_{-1}, t_{-2}, t_1 and t_2 and the SAR features at t_0.

search for the tuning parameters with a tune length of three. They automatically select the best model. Hinton and Salakhutdinov (2006) developed DNNs from Artificial Neural Networks. In deep learning, several blocks of filters or layers with specific functions are stacked to capture image information. This method is increasingly used in remote sensing applications (Li et al., 2019). Using the *keras* R package (Allaire and Cholle, 2021) we built a basic DNN with two dense layers (64 nodes) and *relu* activation with a mean squared error loss function. We trained the model for 100 epochs with a 0.2 validation split and early stopping.

After training the models, we applied the models to the test samples. From the difference between the observed and predicted VIs, we determined the best method by calculating the residual sum (RS), root mean square error (RMSE), and mean absolute error (MAE). Kolecka et al. (2018) found that the NDVI decreases by at least 0.2 after a mowing event. For this reason, we considered deviations of more than 0.2 between observed and predicted values to be particularly critical for the detection of mowing events. If the predicted value differs from the observed value by more than 0.2, the probability of introducing false mowing events or removing real events is high. Therefore, we also used the number of extreme residuals above or below +/−0.2 for evaluation. The method with the lowest RMSE, MAE, RS and number of extreme residuals was then used again to train a model with 100% of all samples with simultaneous S1 and optical data to make use of all available data. This model was applied to the remaining data points of all parcels where SAR data was available, but optical data was missing at t_0 to create a six-day interval of the optical data.

To compare time series fitted to the six-day grid using ML methods and those where missing values were interpolated, we linearly interpolated the original optical data between days of cloud-free acquisitions. Only values that fit the six-day grid were then considered to construct the interpolated time series. We linearly interpolated values between t_{-1} and t_1 (see Eq. (2)) and compared the interpolated VIs with the observed VIs at $t0$.

$$VI(t_0) = VI_{t_{-1}} + \frac{VI_{t_1} - VI_{t_{-1}}}{t_1 - t_{-1}} \cdot (t_0 - t_{-1}) \quad (2)$$

After the gap handling, there were four data sets with time series of satellite and weather features for each grassland parcel on a six-day temporal grid: The three gap-filled ML datasets (RFR, SVR, DNN) and one dataset with linearly interpolated values (*int*). For mowing event detection, only the best gap-filled (*gf*) dataset and the *int* dataset were considered.

We normalized all satellite features of the *int* and *gf* time series from zero to one by parcel and year to scale the input features to the same range of values, as this improves model training (Bisphop, 1995). Weather data were normalized using all weather data from 2017–2019 to preserve the temporal and spatial variability between years and study sites.

3.2. Mowing event detection

To detect mowing events, we sliced the time series of all parcels and features in the six-day grid into sequences of equal length using a sliding window approach, to detect mowing events throughout the whole growing season (see Fig. 5). Five observations before and five after the midpoint t_0 were included in a sequence, resulting in 11 observations over 60 days. This window size was found to be appropriate in Lobert et al. (2021). If a mowing event occurred at the midpoint t_0 or between t_{-1} and t_0, the sequence was labeled as *mown*. If no mowing occurred, or a mowing occurred before t_{-1} or after t_0, it was labeled as *unmown*. We utilized each observation point once as the midpoint t_0 of a sequence.

As described in Section 2.1, some parcels were only valid for training. This was the case when grazing occurred after the mowing. All sequences with coincident grazing were omitted and only sequences before grazing were used for training. The remaining sequences were split into 80% training and 20% test sequences, stratified by year and study site. Each parcel-year combination was considered for either training or testing only. This resulted in approximately 16 000 training and 3 600 test sequences. Of the 16 000 training sequences, 988 sequences and of the 3 600 test samples, 225 sequences included a mowing event. The training set included sequences from 346 extensive, 133 medium and 33 intensive plots.

To classify the sequences into *mown* and *unmown*, we compared four different ML algorithms. Random Forest Classification (RF) and SVM are well-known and established ML classifiers. CNN and Long Short-Term Memory (LSTM) deep learning algorithm have shown great potential in image or time-series classification tasks (Lu et al., 2021; Zhang et al., 2019; Karim et al., 2019). In SVMs, vectors represent each object in a vector space. The SVM fits a hyperplane to this space, which divides the training objects into classes. In order for the hyperplane to separate the objects linearly, the SVM transfers the vectors to a higher dimensional feature space, as in SVR (Vapnik, 2000). As with regression, the RF classification is an algorithm consisting of multiple uncorrelated decision trees. For a classification, each tree in this forest is allowed to make a decision and the class with the most votes decides the final classification. Both RF and SVM do not take into account the order of the features and therefore cannot retain temporal information.

In contrast, CNN and LSTM have the ability to handle the order of the input values. Both are based on Artificial Neural Networks (ANN) with input and output layers and hidden layers in between (Zou et al., 2008). CNN are not designed for time series per se, but are often used in computer vision to detect objects and patterns in images (O'Shea and Nash, 2015). They can be adapted to work on time-series classification (Zhao et al., 2017). A CNN consists of one or more convolutional layers, which extract higher-level features. Within a convolutional layer, the input is transformed by filters before being passed on to the next layer. Initially, the values in the filter are random. Therefore, the first runs, or convolutions, serve as a training phase. After each iteration, the CNN automatically adjusts these values using a loss function. The CNN continuously readjusts the filters as training progresses. Convolutional layers are often followed by pooling layers that summarize and downsample the extracted information (O'Shea and Nash, 2015). LSTMs are recurrent neural networks (RNN) - neural networks that, unlike feedforward networks, are characterized by connections from neurons in one layer to neurons in the same or a previous layer (Hochreiter and Schmidhuber, 1997). RNNs keep track of arbitrary long-term dependencies in the input sequences that can provide contextual information. This makes them ideal for time series

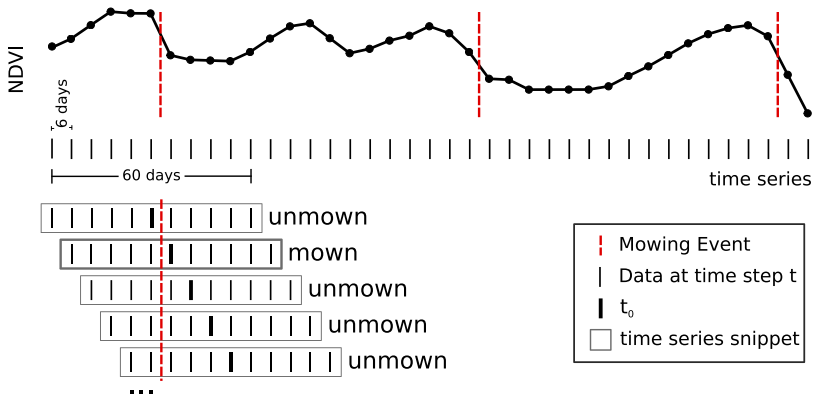

Fig. 5. Division of time series into time series sequences. Sequences were labeled as *mown* if mowing occurred in the period between t_{-1} and t_0 or on t_0.

classification and prediction. But a vanilla RNN is trained using back-propagation, thus the long-term gradients that are back-propagated can "vanish" and tend to zero, or "explode" and tend to infinity, forgetting or overemphasizing information from long ago. LSTM units, which also allow gradients to flow unchanged, prevent this problem. An LSTM cell consists of three parts: The first part is the *Forget Gate*, which remembers or forgets information from previous time steps. The second part (*Input Gate*) learns new information from the current input and the third part is the *Output Gate*. This gate passes the updated information to the next cell. The cell knows the *hidden state* of the previous and the current state, which can be seen as a short-term memory. Unlike RNNs, LSTMs also know the state of the cell. This is the long-term memory that carries information with all time steps. For a deeper insight into CNN and LSTM see Goodfellow et al. (2016).

For the RF and SVM methods, we used the *caret* package in R (Kuhn et al., 2021). The aim of our study was not to perfect one method but to compare the general ability of the approaches to determine grassland use intensity. Therefore, we used the default classification settings for RF and SVM. Both resample five times k-fold and use an automatic grid search for the tuning parameters with a tune length of three. We implemented the CNN and LSTM methods with *Keras* and *TensorFlow* backend in R (Fabel et al., 2022; Kalinowski et al., 2023). We used the same CNN model as used in Lobert et al. (2021), who adapted a 1D-CNN from Wang et al. (2017). It consists of two convolutional layers with kernel sizes of five and three, respectively. The output of the convolutional layers was zero-padded to remain the same size as the input. Batch normalization and a rectified linear unit (ReLU) activation function were applied after each layer. The two convolutional layers were followed by a global average pooling and a single densely connected and sigmoid-activated neuron to give the final output. The LSTM model was again a stacked LSTM consisting of two LSTM layers (24 and 48 units respectively) followed by a dropout layer to prevent overfitting and a dense layer with sigmoid activation at the end. The *binary crossentropy* with *rmsprop* optimizer was used as a loss function. We trained 100 epochs with a batch size of 64 and a validation split of 0.2. The training curves were controlled randomly to avoid overfitting.

The binary classification task is very unbalanced with only 5% *mown* samples (n = 1 285) compared to 94% *unmown* samples (n = 23 866). In this case, ML algorithms may be biased towards the larger group. To balance out the dataset, we up-sampled the *mown* samples using the random oversampling method (Ling and Li, 1998) until they reached the same sample size as the *mown* samples. This was done using the *upSample*-function of the R *caret*-package. All the original data were left intact and additional samples were added to the minority classes with replacement. Random upsampling proved to be the best method for this task in previous experiments, compared to downsampling the *unmown* samples, creating artificial samples with the Synthetic Minority Oversampling Technique (SMOTE) (Chawla et al., 2002), or using weighting factors on the samples. We then tested the four classification algorithms in multiple runs with different settings. We ran the sequences generated by the best ML *gf* method against the *int* time series, each with six different feature combinations. With the different feature combinations, we tested how the method behaved with only optical or only SAR data, and what the influence of the weather was (see Table 3 and Section 2.4).

We then tested the same combinations for transferability. To test spatial transferability, we manually separated training and test data by study site, ensuring that the training and test datasets included different intensity levels and spatial locations within Germany. We used all sequences from Aulendorf (medium-intensive; southern Germany), Lindhof (extensive-medium; northern Germany), Schorfheide-Chorin (extensive; north-eastern Germany) and Schwäbische Alb (extensive-medium; southern Germany) for training, and tested the models on the sequences from Hainich (extensive, central Germany), Haus Riswick (medium; western Germany), and Trenthorst (extensive; northern Germany). To test the temporal transferability, we trained the model on two of the three years and tested it on the remaining year — each of the years 2017–2019 was the target year once.

Mowing events were often detected in successive sequences because the characteristics of a mowing event are present although not at t_0 (Lobert et al., 2021). Therefore, consecutive classified mowing events were clustered to the median event with a tolerance of +/−12 days. The classification results of the different methods and feature combinations were then compared in terms of precision (true positive rate — TPR), recall (positive predictive value — PPV) and F1-score (F1), which is the harmonic mean of precision and recall (Kent et al., 1955).

In addition, we analyzed the ability of the models to find the exact number of mowing events per parcel and the number of correctly classified first two mowing events in the test dataset. For the latter, in addition to the condition that the mowing event must be within a tolerance of +/−12 days, it must also be in the correct position/order; for example, a second cut is only valid if the date is correct and there is only one cut detected before that date.

4. Results

4.1. Gap handling

We tested the ability of three different ML methods and linear regression to predict optical data at dates with only SAR data. The results showed that all methods, including linear interpolation, predicted gaps within the VI time series mainly within the non-critical range of residuals between −0.2 and 0.2 (see Fig. 6). The medians of the residuals were close to zero, and the lower and upper quartiles were narrow for all methods. For the mowing event detection, we, therefore, focused on the ability of the approaches to avoid extreme residuals with residuals below or above this range. For both NDVI and EVI, the

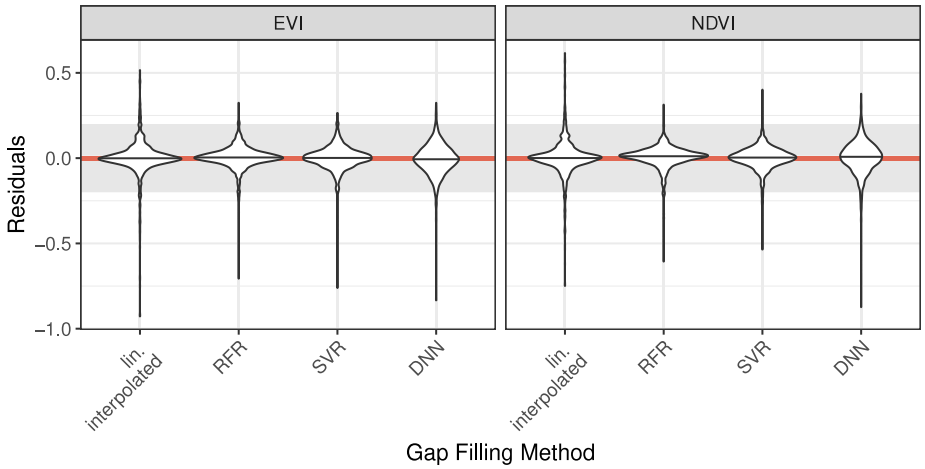

Fig. 6. The residual distribution of the Gap-handling results calculated with DNN, SVR, RF, and with linear interpolation. The differences between observed and predicted values are shown (residuals). The light-grey area marks the residual range between −0.2 and 0.2, which is considered to be non-critical for mowing event detection.

Table 4
Metrics for gap handling algorithms by vegetation index and algorithm. Extreme Residuals are the number of values with residuals larger than 0.2 or lower than −0.2. The best results are shown in bold.

VI	Algorithm	RMSE	MAE	Extreme residuals	Residual sum
NDVI	interpolated	0.102	0.061	87	95.34
	RFR	**0.069**	**0.044**	**34**	**69.3**
	SVR	0.07	0.047	36	73.93
	DNN	0.091	0.063	53	99.07
EVI	interpolated	0.101	0.057	86	88.56
	RFR	**0.069**	**0.044**	36	**68.53**
	SVR	0.071	0.048	**31**	75.54
	DNN	0.099	0.067	58	104.6

interpolation produced the highest number of extreme residuals. RFR and SVR resulted in the lowest number of critical extreme residuals for NDVI and EVI, respectively (see Table 4). RFR gave the lowest RMSE, MAE, and RS values for NDVI and EVI with RMSE = 0.072 and 0.070, MAE = 0.048 and 0.047, and RS = 69.30 and 68.53 respectively. Compared to the other methods, the DNN had the highest interquartile range and was the least suitable for filling the gaps.

Fig. 7 shows the gap-filled and interpolated time-series for three randomly selected parcels in the year 2017 on the six-day grid together with the actual NDVI values on the day of acquisition. In most cases, the RF and SVR predictions capture the trends quite well. In contrast, the DNN time-series show large fluctuations. In Aulendorf and Schwäbische Alb low values are moderated compared to the real values. This can lead to mowing events not being detected, but low values due to undetected clouds can be compensated (see very low value around September in Aulendorf). In Trenthorst there were only few optical scenes available throughout the year. The interpolated time-series is therefore very flat. The ML algorithms introduce more movement.

As the RFR algorithm had the lowest RMSE, MAE, and RS values and the lowest number of extreme residuals for NDVI, we used it to continue with the Gap-handling. An analysis of the variable importance of the RFR model showed that for both VIs, the most important variables were the optical variables themselves immediately before and after the gap (70.6 and 56.7). VV and VH coherence at t_1 (3.5 and 2.9) and backscatter RVI at t_0 (2.3) had the highest variable importance of the SAR features, but they have a comparatively low importance. The time between optical acquisitions did not play a role.

4.2. Mowing event classification

Mowing event detection was performed with different settings to find the best algorithm, the best feature combination, and the best Gap-handling method for classifying time series sequences into *mown* and *unmown*. We tested two different methods to generate missing optical data in temporal grids, four different ML methods for classifying time series sequences, and six different feature combinations. Correctly classified mowing events were within a tolerance of +/−12 days of the reference mowing date. We evaluated the results with F1, PPV, and TPR. Fig. 8 shows in (a), (b), (c) and (d) the results separated by gap handling, algorithm, and feature combination, as well as the results by year. Table 5 shows the ranking of all classification settings ordered by F1. The best classification result was obtained with *gf* time series with optical and weather features (*OPT+W*) and the LSTM algorithm (TPR = 0.92, PPV = 0.85, and F1 = 0.89).

Fig. 8(a) breaks down the by the ML algorithm. CNN and LSTM produced robustly good models with high medians and narrow interquartile ranges for F1, PPV and TPR. RF tend to produce rather poor models, with F1 and TPR varying widely from model to model. The SVM models also had narrow interquartile ranges but do not achieve as high F1, PPV, and TPR values as the CNN and LSTM methods. Due to the unreliable results of RF and SVM, Figs. 8(b) to 8(d) show only the results of LSTM and CNN. Fig. 8(b) compares the results of the mowing event detection for time series with linearly interpolated VIs (*int*) and for time series with gap-filled VIs (*gf*). The median F1, PPV, and TPR were very similar for both gap filling methods, with the *int* values being slightly better.

The overall best model in terms of F1 used optical and weather data, but no SAR features (*OPT+W*). The combination of *OPT+W* features also gave stable results (see Fig. 8(c)). Among the top ten models, where the values are close overall, there are only variations with optical (*OPT*) and optical and SAR features combined (*OPT+SAR*). Except for one case, these models always included weather data (*OPT+W* or *OPT+SAR+W*). From Fig. 8(c) it is clear that weather data improved the classification results.

We analyzed the results to see if there were differences in predictive power across use intensity levels (see Fig. 10). The best results were obtained for the intensively used parcels with a median F1 of 0.93, followed by the medium intensity parcels (F1 = 0.88) and extensive parcels with F1 of 0.67 based on the LSTM and CNN algorithm. We differentiated by individual parcel because the use intensity of one study site differed for individual parcels. The training set included 7800 sequences from extensive parcels, 7000 samples from medium intensive parcels, and 1150 samples from intensive parcels.

Looking at the different test sites, the best results were obtained at the Riswick test site, followed by Schwäbische Alb and Aulendorf with median F1 values of 0.94, 0.83 and 0.80 respectively. These were the study sites with the most sample sequences in the training data set —

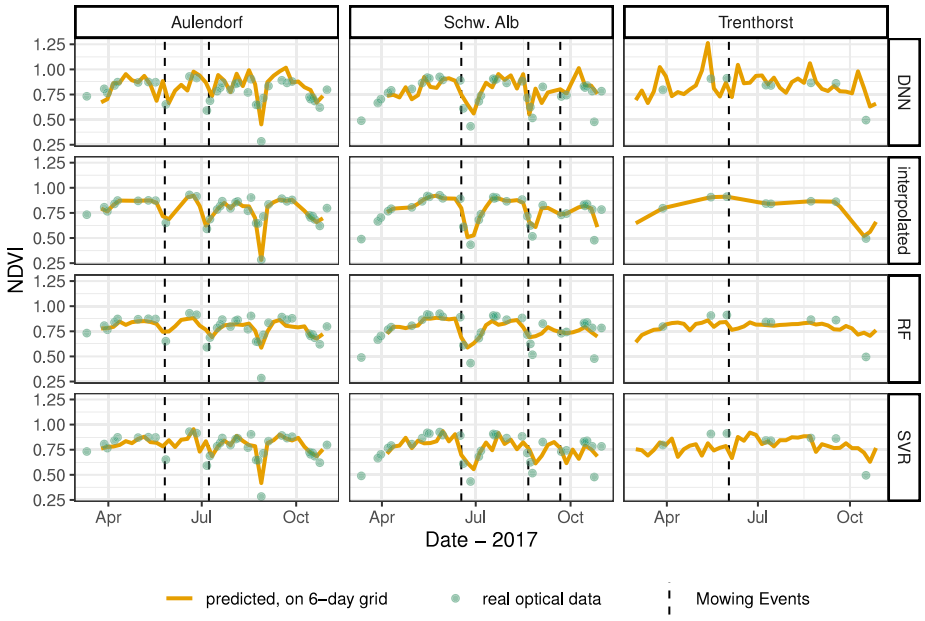

Fig. 7. Actual and predicted NDVI values from DNN, linear interpolation, RF, and SVR for three parcels of three study sites for the year 2017. Predicted values were predicted on the 6 day grid.

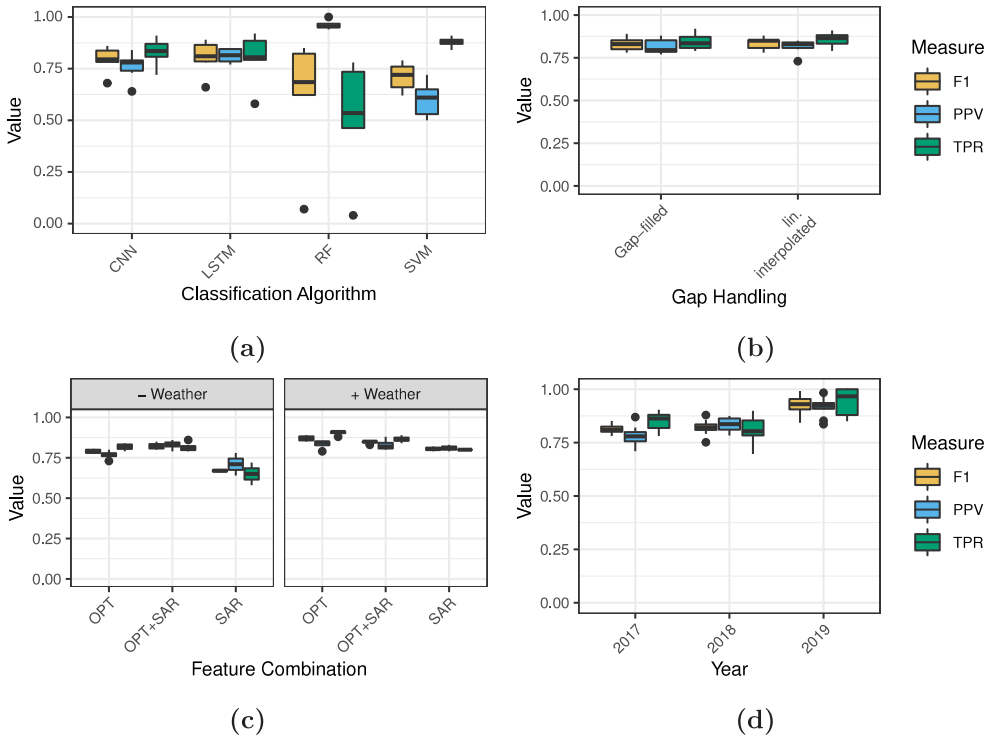

Fig. 8. Classification measures F1, Precision (PPV) and Recall (TPR) for time series sequence classification into *mown* and *unmown*. (a) shows the results for the classification algorithm, (b) depicts the results grouped by gap handling method without SAR models, (c) the results grouped by feature combination, and (d) discriminated between years. In each case, all results were taken into account and only subdivided according to the corresponding category. (b) - (d) only include the CNN and LSTM algorithm.

over 3000 each. The results for the other study sites with less than 2000 sample sequences reached median F1 values of 0.64 (Schorfheide) or 0.67 (Lindhof, Trenthorst and Hainich).

For those mowing dates that were correctly identified within the +/−12 day evaluation window, the difference between the predicted and actual mowing dates for the LSTM and CNN models was on average only two days earlier than the predicted date. The mean MAE was 2.6 days and the mean RMSE was 4.0 days when comparing the predicted date with the actual date.

We also looked at the results for the three years considered (see Fig. 8(d)). 2019 had the best classification results. 2017 and 2018 both had worse results, with 2017 having better TPR and 2018 having better PPV values. The higher TPR values in 2017 indicate that cuts were more likely to be missed, whereas in 2018 mowing events were detected, that did not take place.

Table 5
Classification metrics for mowing event classification by algorithm, gap handling and features. F1, Recall (TPR) and Precision (PPV) are shown. The list is ordered by descending F1.

Method	Gap handling	Features	Weather	F1	PPV	TPR
LSTM	Gap-filled	OPT	+ W	0.89	0.85	0.92
LSTM	Lin. interpolated	OPT	+ W	0.88	0.85	0.91
CNN	Lin. interpolated	OPT	+ W	0.86	0.84	0.88
LSTM	Gap-filled	OPT+SAR	+ W	0.86	0.88	0.84
CNN	Gap-filled	OPT	+ W	0.85	0.79	0.91
CNN	Lin. interpolated	OPT+SAR	−W	0.85	0.84	0.86
CNN	Lin. interpolated	OPT+SAR	+ W	0.85	0.81	0.89
LSTM	Lin. interpolated	OPT+SAR	+ W	0.85	0.83	0.87
RF	Gap-filled	OPT	+ W	0.85	0.95	0.78
RF	Lin. interpolated	OPT	+ W	0.85	0.94	0.78
CNN	Gap-filled	OPT+SAR	−W	0.83	0.86	0.80
CNN	Gap-filled	OPT+SAR	+ W	0.83	0.80	0.86
LSTM		SAR	+ W	0.82	0.83	0.80
LSTM	Lin. interpolated	OPT+SAR	−W	0.81	0.83	0.79
CNN	Gap-filled	OPT	−W	0.80	0.77	0.83
LSTM	Gap-filled	OPT+SAR	−W	0.80	0.79	0.81
LSTM	Lin. interpolated	OPT	−W	0.80	0.80	0.81
CNN		SAR	+ W	0.79	0.79	0.80
SVM	Gap-filled	OPT	−W	0.79	0.72	0.88
CNN	Lin. interpolated	OPT	−W	0.78	0.73	0.84
LSTM	Gap-filled	OPT	−W	0.78	0.77	0.79
SVM	Gap-filled	OPT+SAR	−W	0.78	0.67	0.93
SVM	Gap-filled	OPT	+ W	0.76	0.65	0.91
SVM	Gap-filled	OPT+SAR	+ W	0.75	0.64	0.92
RF		SAR	+ W	0.74	0.96	0.60
SVM	Lin. interpolated	OPT+SAR	−W	0.74	0.61	0.92
RF	Lin. interpolated	OPT+SAR	+ W	0.73	0.98	0.58
RF	Gap-filled	OPT+SAR	+ W	0.72	0.97	0.58
SVM	Lin. interpolated	OPT	+ W	0.72	0.61	0.89
SVM	Lin. interpolated	OPT+SAR	+ W	0.72	0.61	0.89
CNN		SAR	−W	0.68	0.64	0.72
LSTM		SAR	−W	0.66	0.78	0.58
SVM		SAR	+ W	0.66	0.53	0.87
RF	Lin. interpolated	OPT	−W	0.63	0.97	0.46
RF	Gap-filled	OPT	−W	0.62	0.95	0.47
SVM		SAR	−W	0.62	0.50	0.84
RF	Gap-filled	OPT+SAR	−W	0.28	0.97	0.16
RF	Lin. interpolated	OPT+SAR	−W	0.25	1.00	0.14
RF		SAR	−W	0.07	1.00	0.04
SVM	Lin. interpolated	OPT	−W	NA	NA	0

To determine whether the length of the gaps between optical scenes affected the classification result, we calculated the median number of days between acquisitions per year and study site. We plotted the F1 values for all parameter combinations containing optical data against the median gap sizes (see Fig. 9). The *SAR* model was excluded because gaps in the optical data do not affect the SAR data. We also calculated the Pearson correlation. There is a negative correlation between F1 and gap length for median gaps of ten days or more (r = −0.44). This effect is largely due to the poor results for median gaps of 20 days, caused by a parcel in the Trenthorst study area in 2017. Excluding gap lengths of 20 still resulted in a negative correlation with r = −0.26. The negative correlation does not occur for results with median gaps smaller than ten days (r = 0.08).

4.2.1. Transferability

Training and testing the algorithms on independent datasets – either temporally or spatially – still gave good performance, although the ability of the algorithm to detect mowing events in the test data deteriorated (see Fig. 11 and Tables A.6–A.9). Overall, the F1 score varied between 0 and 0.79 for all models and gap handling methods.

CNN was the best overall algorithm (see Fig. 11(a)). RF was not able to reliably predict mowing events and gave the worst results. Although the SVM algorithm sometimes gave good and even better results than LSTM, it lead to zero mowing event detection rate for some feature combinations. The results for gap filling were still inconclusive (see Fig. 11(b)). Although the *gf* models gave the best results, *int* models were more reliable. Feature combinations without weather data (-W) gave better results than those with weather data (+W) (see Fig. 11(c)(c)). Models including both optical and SAR data were generally superior to *OPT* or *SAR* models, with the *SAR* model being the clearly worse of the two. Nevertheless, the best CNN models did not need SAR data.

Spatially independent mowing events were best identified with the CNN algorithm and the *OPT +W* and *gf* model (F1 = 0.76) (see Fig. 12 and Table A.6). Extrapolation to independent years could be best achieved with CNN, *OPT+SAR -W* and *gf* time series for the target year 2017 (F1 = 0.72, see Table A.7); CNN, *OPT -W* features and *gf* time-series for the target year 2019 (F1 = 0.79, see Table A.9); and CNN, *OPT-W*, *gf* for the target year 2018 (F1 = 0.72, see Table A.8). The TPR was always higher than the PPV for the spatially independent models and the temporally independent target year 2017, meaning that the models tend to miss true positives. For the target years 2018 and 2019, the PPV was mostly higher than the TPR. Thus, more true positive mowing events were detected but also more false positives.

We tested the spatially independent data on the three test sites Hainich (extensive), Riswick (medium intensive) and Trenthorst (extensive). The best results were obtained for Riswick and Hainich with mean F1 = 0.70 and F1 = 0.64 respectively. Trenthorst only achieved a mean F1 = 0.51. The evaluation of spatially independent years again showed that the results for 2017 (mean F1 = 0.66) were worse than for 2018 (mean F1 = 0.75) and 2019 (mean F1 = 0.70).

4.2.2. Intensity estimation

The intensity of grassland use can be defined by several factors related to mowing events, such as the number of cuts, the recovery time between cuts, or the timing of the first cut. The first two cuts and the total number of cuts per parcel are considered to be the most important factors in estimating the use intensity, while the timing of the first cut is also important for environmental measures. In this section, we focus on analyzing the temporal and spatial accuracy of the first two cuts and the number of cuts per plot.

Fig. 13 illustrates the accuracy of the LSTM algorithm in predicting the number of mowing events per parcel compared to the actual number of mowing events. Overestimation and underestimation are shown, differentiated by the number of actual mowing events. A further distinction is made between the methods used to manage the gaps. The figure shows that areas mown once or twice a year tend to be overestimated, whereas sites mown more frequently tend to be underestimated. While the number of over- or underestimations was generally limited to one or two events, some exceptions were observed with differences of up to four cuts. The MAE for the number of mowing events for all parameter combinations for LSTM and CNN was 0.67. The best overall model *OPT +W* achieved a MAE of 0.47.

The *SAR +W* feature combination was found to be the best predictor for plots with only one mowing operation per year, while the *OPT +W* and *OPT -W* models with *gf* time series performed well in identifying the correct number of cuts on two-cut meadows. The *OPT +W - gf* model gave the best results on three-cut and four-cut meadows. Although the *OPT +W - gf* model identified all mowing events on five-cut parcels, the data for such parcels were underrepresented in the data, and therefore the results cannot be considered representative.

The correct detection of the first mowing event can already indicate the use intensity of grassland by its date. The time between the first and the second mowing events can also indicate the use intensity.

We analyzed the number of correctly classified first two mowing events in the test dataset (see Fig. 14). The figure shows the number of correctly classified mowing events by feature combination and the cut position for the LSTM method and the gap-filled time series. The first mowing events were correctly classified with 67% to 94%. The run with *OPT +W* reached 94%. Both *OPT + SAR +W* and *OPT + SAR -W* reached 88%. Again, there is no significant difference between the *gf* and *int* models. The second mowing event of each parcel was less

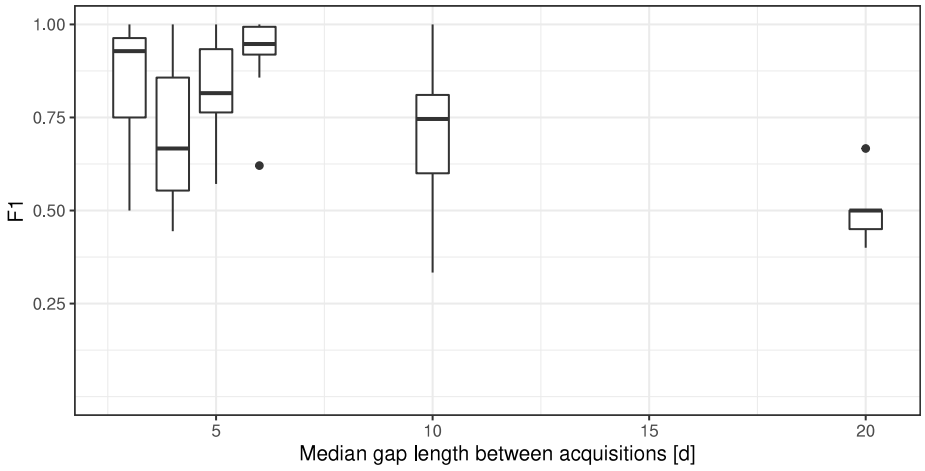

Fig. 9. Influence of the gap length between optical acquisitions on the classification results represented by the F1 measure per year and study site of classifications. The results for all parameter combinations that include optical data are shown.

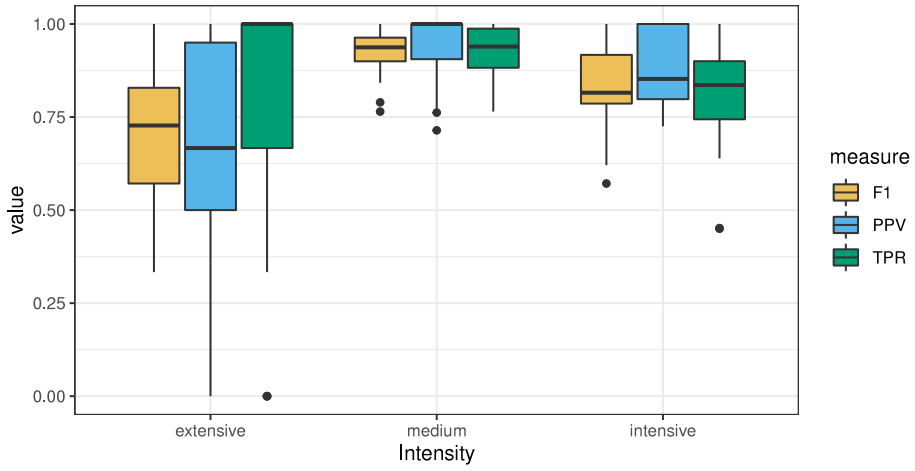

Fig. 10. Classification results by intensity of study site.

often correctly classified, with a maximum of 71% correctly classified (*OPT +W* and *int*).

On all study sites, the first mowing event could be correctly classified by at least 67% for *OPT + SAR +W* and *gf*. For the second mowing the results were different. In the Hainich and Schorfheide areas, less than 25% of the second cuts were found to be in the correct position. Aulendorf, Lindhof and Schwäbische Alb achieved 52–57% and in Riswick 80% of the second cuts were correctly detected. The results were not significantly different over the three years.

5. Discussion

5.1. Gap handling

Throughout the analysis, we compared whether there was an advantage to infilling the optical vegetation index time series with a machine learning approach rather than linearly interpolation. We used harmonized S2 and L8 data. The joint use of two sensors already increases the availability of satellite data compared to single sensor approaches (Moreno-Martínez et al., 2020; Claverie et al., 2018). Filling the remaining gaps with machine learning resulted in a slight advantage of the predicted values over the interpolated values in the direct comparison between the approaches. NDVI MAE of 0.044 and RMSE of 0.069 for NDVI were comparable to the results of the RNN of Garioud et al. (2021) for grassland sites with MAE of 0.042 or 0.044 and RMSE of 0.061 or 0.063 for their two sites. The threshold of 0.2 residuals is based on the assumption that this is the minimum deviation that indicates a cut (Kolecka et al., 2018). However, Schwieder et al. (2022) pointed out that thresholds are often not static, but should be dynamically adjusted for years and grassland parcels. We also created the gaps artificially by removing values from the time series. As a result, the gaps created were longer than those actually present in the data. For these reasons, relying solely on the extreme residuals to evaluate the gap filling methods is less robust than analyzing the value of the two mowing event detection methods.

Further analysis showed that there was no systematic advantage of the RFR-filled time series for the detection of mowing events. We expected to find a clear difference when comparing the results by year, as the availability of optical satellite imagery varies between years. There were sometimes longer gaps in the critical periods of May and June — especially in 2017, a very wet year. We also assumed that linearly interpolated time series would result in missed mowing events if the gaps were too long (Buddeberg et al., 2016; Reinermann et al., 2022). However, the differences between interpolated and filled time series were often minimal in the mowing event detection results. The TPR values, which can be an indicator of missed mowing events, were also not very different. Due to the combined use of L2 and L8, the median period between acquisitions only reached 20 days for Trenthorst in 2017. Further studies on reference data with longer gaps are recommended, also considering the study by Schmidt et al. (2014) who found that the timing of satellite imagery can be crucial for grassland related studies. Overall, our study suggests that interpolated

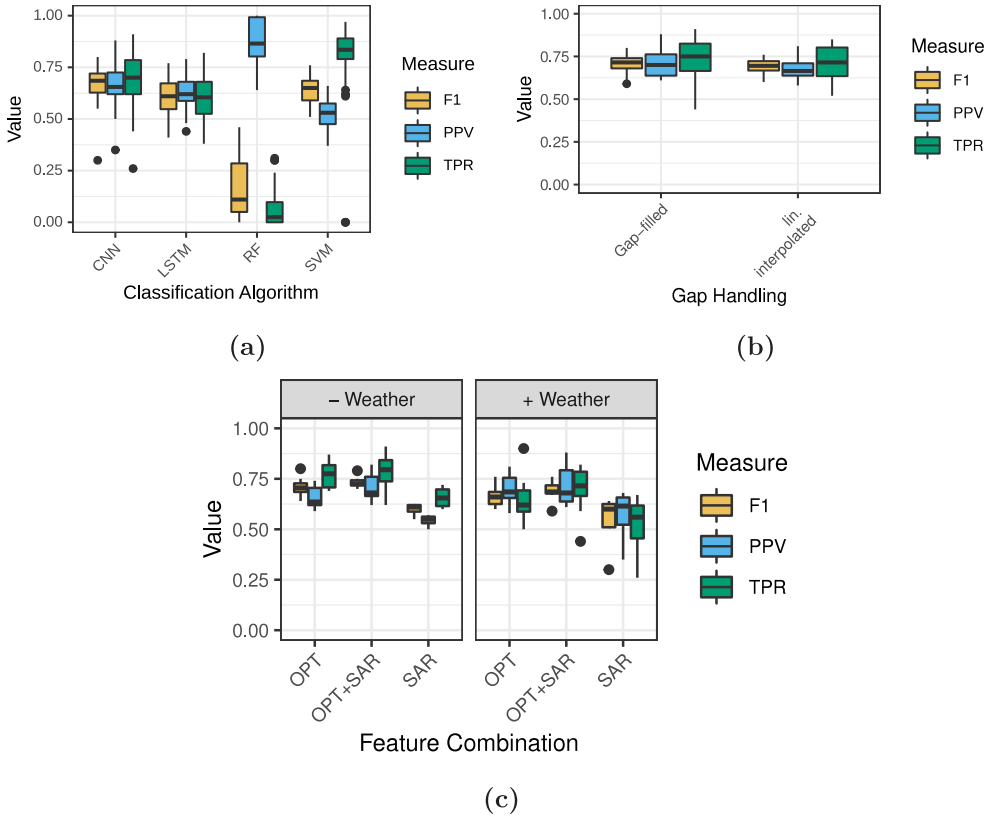

Fig. 11. Classification measures F1, Precision (PPV) and Recall (TPR) by different factors for classifying time series sequences into *mown* and *unmown* for spatially or temporally separated training and test data sets for extrapolation to unknown years or locations. In each case, all results were considered and only subdivided according to the corresponding category. (b) and (c) include only the CNN algorithms. (a) shows the results for the classification algorithm, (b) shows the results grouped by gap handling method without the pure SAR models, and (c) shows the results grouped by feature combination.

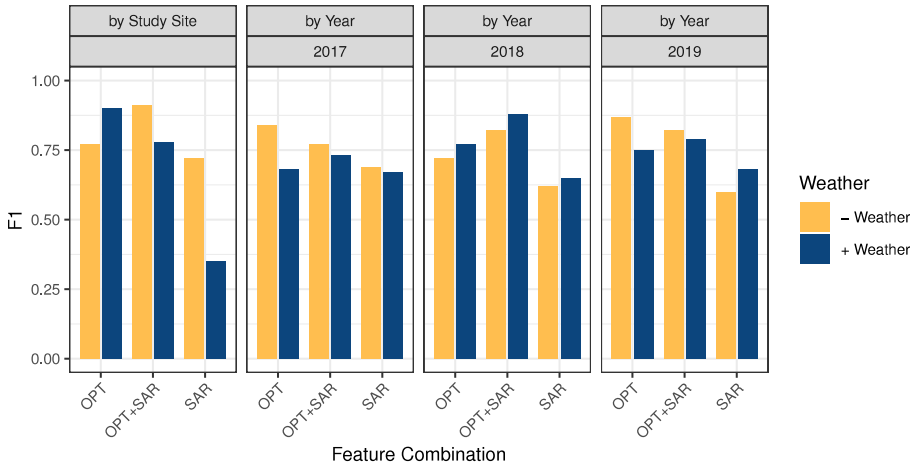

Fig. 12. Classification measures F1 for time series sequence classification into *mown* and *unmown* for the CNN method by parameter for spatially or temporally separated training and test data sets for extrapolation to unknown years (by Year) or locations (by Study Site). The years shown are the years in the test data set.

optical time series from two different sensors could be sufficient to detect mowing events in Germany. This is an advantage for area-wide and recurrent application, as it is much easier to implement than a two-step procedure with an upstream filling of gaps in the time series. When developing classification algorithms with the aim of ensuring their transferability over space and time, the goals of robustness and simplicity are often sought alongside accuracy (Halabuk et al., 2015). Nevertheless, we have not considered algorithms that can use the time dimension or consider the order of variables for gap filling. These may be more advantageous, as shown by Garioud et al. (2020, 2021).

5.2. Mowing event detection

Overall, our mowing event detection in time series sequences was very successful. When both training and test data included all study sites and years, the results were excellent. Optical data outperformed

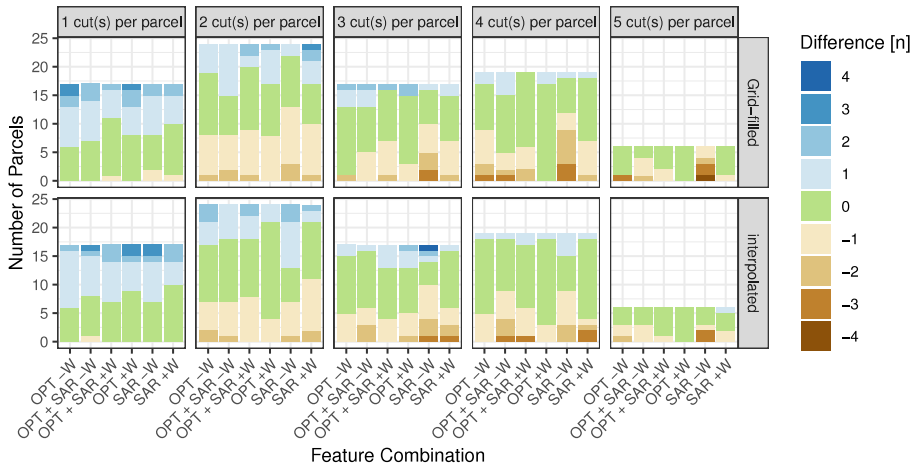

Fig. 13. Difference between the reference and predicted number of mowing events per parcel by method, feature combination (−W: without weather features, +W: including weather features) and total number of cuts per year per parcel. The results for the LSTM algorithm are shown. Positive differences indicate an overestimation of the frequency and negative differences an underestimation.

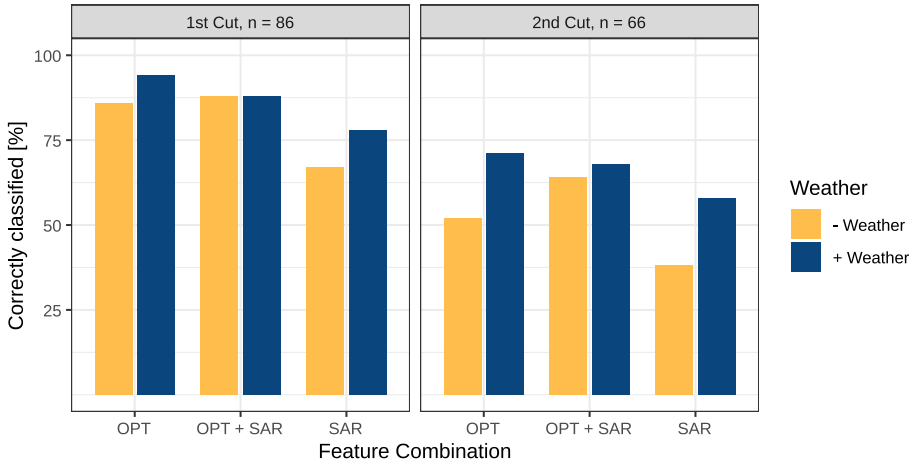

Fig. 14. Share of correctly classified mowing events by their correct date and correct position with the LSTM method and gap-filled time series. The suitability of the different feature combinations for the first and second mowing event is presented.

the combined use of optical and SAR data, and weather data supported the classification. However, when the model was extrapolated to years or areas not included in the training data, the results deteriorated slightly. In terms of model transferability, SAR data improved the detection of mowing events, while weather data worsened the results.

Our models achieved F1 values of up to 0.89, which is even higher than the highest F1 values of 0.84 achieved by Lobert et al. (2021), 0.83 achieved by Halabuk et al. (2015) or 0.80 achieved by Taravat et al. (2019). Even with a smaller tolerance window of three days before and 12 days after the actual cut, which is the same as in Schwieder et al. (2022), the F1 values only decreased by about 0.05. These results show that this approach is a valuable step towards CAP control during the season.

For the detection of mowing events, the *OPT* models without SAR data were superior to the other options in terms of detection quality and robustness of results for models trained on all parcels and years. This contradicts the results of Lobert et al. (2021), who found improvements with the joint use of optical and SAR data. However, Reinermann et al. (2022) also found that the use of optical data alone was better for detecting mowing events. Some studies support that SAR backscatter (Voormansik et al., 2020; Zalite et al., 2016) or coherence shows no or at most an ambiguous relationship with mowing events (Zalite et al., 2014; Reinermann et al., 2022). Other studies find backscatter (Grant et al., 2015b; Taravat et al., 2019) or coherence useful (de Vroey et al., 2021). The good results of optical data have been often stated in literature, which widely acknowledges that optical remote sensing is useful for detecting abrupt changes in vegetation condition (Kolecka et al., 2018; Estel et al., 2018). Although not part of the study, we looked at the use of backscatter and coherence data alone for comparability. The results were very similar to those of Lobert et al. (2021), with coherence being superior to backscatter when considered alone. The combined use of backscatter, coherence and optical data (OPT+SAR) was worse than optical and coherence or optical and backscatter.

Weather data positively influenced the classification results when rolling temperature and precipitation sums were included in the mowing event detection classification, but only when the training data included all study sites and years. Weather data is the same for all parcels of a study site. Therefore, it is possible that they can be used as grouping factors and contextual information for the parcels, which is likely to improve the results (Li et al., 2014). Both precipitation and temperature influence biomass development and thus the time slots

when grassland cuts are most beneficial (Smit et al., 2008). Precipitation can also determine when mowing is inappropriate, as grass is usually cut only on days without precipitation.

In a comparison of algorithms for mowing event detection, CNN and LSTM were far superior to the more traditional methods RFC and SVM. They can take into account the temporal order of values (Zhao et al., 2017). Compared to Lobert et al. (2021), our CNN model results were more stable for different feature combinations, even though it was the same CNN algorithm with the same configurations. This may be due to the use of more ground truth data in this study. Although often suitable for remote sensing tasks (Belgiu and Drăgu, 2016), the RF algorithm did not produce consistently good results. However, both the RF and SVM models were rather simple models and it may be possible that parameter tuning could improve the results.

The results varied according to the regions studied and the intensity of use. This can also be seen in the studies of Lobert et al. (2021) or Schwieder et al. (2022). On intensively used parcels we obtained better results. Plots with less frequent mowing are also more likely to have unrecorded grazing. Grazing can have a large effect on the signal and thus lead to false results (Dusseux et al., 2014a; Reinermann et al., 2022). In addition, senescent biomass is more common in autumn on more extensive sites and can cause distortions in the signal (Holtgrave et al., 2020b). The results also varied between study sites. There is evidence that sample size may have played a role, as there was significantly more training data for the sites with the best results. This phenomenon is known from classification tasks with classes of different sizes (Bogner et al., 2018; Blickensdörfer et al., 2022).

Classification results differed between years, even when the models were trained on data from all years: 2017 results were the worst and 2019 results were the best. This was also the case for Lobert et al. (2021). Schwieder et al. (2022) also found overall better F1 scores for 2019 than for 2018 in Germany. When extrapolating from specific years to unknown years, the results were worst for the target year 2018 and best for the target year 2019. 2017 was a wet and cloudy year. High soil moisture levels could have caused signal interference. Undetected clouds in the data could have led to false positive classification of mowing events (Griffiths et al., 2019). The inferiority of the 2017 results may also be due to the size of the gaps between two acquisitions, due to persistent cloud cover. The median gap size for 2017 is mostly greater than or equal to ten days. Our results indicate that the median gap size and F1 as a measure of classification are not correlated below a median gap size of about 10 days. Only for larger gaps we observe a negative correlation. However, as our sample contains hardly any observations with gaps of more than 10 days, this statement should be treated with caution. In contrast to 2017, 2018 was a very dry year. In many places, grassland vegetation did not regrow much after the first cut. Differences in grass height before and after each subsequent cut may therefore have been small and therefore difficult to detect. This may have worsened the results compared to 2019, which was a relatively normal year in terms of weather conditions.

The definition of use intensity of permanent grassland is ambiguous. Definitions are not universally accepted, as the same number of mowing events can be considered extensive or intensive depending on the region in Germany and the respective yield potential based on soil type and altitude, among other factors. In addition, the timing of management is weather dependent and can therefore change from year to year. The exact weather conditions at the beginning of the year have a very large influence on the first mowing date as well as on the time between mowing events (Schoof et al., 2020). The number of mowing events, which determines the intensity of use, varies regionally due to different environmental conditions. Therefore, we classified the number of events or the date of the first mowing event without assigning a use intensity. We showed that the number of mowing events was mostly overestimated, which could also be due to unreported grazing activity (Reinermann et al., 2022). Information on grazing could improve the models. The overall MAE for the LSTM and CNN models was 0.67, which is slightly higher than reported in Lobert et al. (2021), who reported MAEs between 0.32 and 0.42 for parcels mown one to three times and 1.44 for parcels mown four times. Our best model (*OPT +W*) achieved an MAE comparable to that of MAE = 0.47.

The LSTM models were able to detect the first cut with an accuracy of up to 94%, allowing a tolerance of +/−12 days for correct classification. Detection of the second cut was less reliable. The first cut was best detected because the greatest difference in biomass occurs between before and after the mowing (Dusseux et al., 2014b). This leads to the most significant changes in the remote sensing signals. Later, the grass height before and after the mowing events differs less. The timing of the first mowing is important for biodiversity and forage production, as well as for CAP compliance. The perfect timing for forage production and biodiversity is very much dependent on phenology and thus on the weather. In years with a cold spring or long periods of almost daily rainfall, farmers may cut even very intensive meadows for the first time a month later than in normal years. The recovery period between the first and second mowing can also be very weather dependent. Its length determines which plant species are able to regrow and recover, and thus the species composition of the area in the long term (Smit et al., 2008).

Transferability is not often tested in mowing event detection studies. In this study, the best models achieved high F1 scores between 0.72 and 0.79 for temporally or spatially independent training and test datasets. These results are still competitive with other studies that did not test for transferability.

There were no clear results regarding the best model parameter for the transferability tasks. Intensity of use had no significant effect on the results of the spatial transferability task. Trenthorst performed the worst, presumably because of larger gaps within the time series (Schwieder et al., 2022). The very best models for transfer to new study sites or to 2018 or 2019 used only optical data, but the best model for 2017 included optical and SAR data, and median F1 values were higher for OPT+SAR than for OPT. The value of joint optical and SAR data for mowing detection has been demonstrated in some studies (de Vroey et al., 2022; Lobert et al., 2021). As transferability is important for periodic monitoring of grassland, we conclude that SAR features should continue to be considered for mowing event detection. However, the S1-B satellite stopped providing data since December 2021, extending the SAR time grid to 12 days. Whether this is still sufficient to complement optical data for mowing event detection needs to be investigated.

The advantages or disadvantages of weather data for transferring models to unknown years or locations were also inconclusive. Transferring models to the years 2017 and 2019 usually worked better without weather data. This could be because all three years from 2017 to 2019 had very different weather conditions, making the information less useful. The benefit of weather data for extrapolation to unknown study areas depended on the satellite data used. When *OPT* models were used, weather data were helpful, but when *OPT+SAR* models were used, they were useless. This was unexpected as it was assumed that weather data would improve the results, especially when combined with SAR data (Zalite et al., 2014; Garioud et al., 2021). But adding more features with low explanatory potential can introduce more noise and decrease the results.

6. Conclusion

In conclusion, this study demonstrates the reliable detection of mowing events throughout the growing season using CNN and LSTM models applied to optical and SAR satellite time series data. These models exhibit high accuracy, even for areas and years not included in the training dataset. While LSTM performs slightly better on known study sites and years, CNN shows superior transferability. The detection of the first mowing event with high accuracy highlights the relevance of

this research for grassland monitoring tasks outlined in European and German agricultural and environmental policies.

Furthermore, our findings suggest that advanced gap filling methods may not be necessary for time series analysis in Germany when using both L8 and S2 images. The impact of different gap handling methods, such as linear interpolation and random forest gap filling, was minimal and can be disregarded. This practical advantage allows for widespread application, saving both processing time and computing power.

Regarding feature selection for mowing event detection, the literature lacks consensus, and our study reaffirms this ambiguity. The choice of feature combination depends on whether the model is applied to known data in terms of time and space or for transferability. Optical data proves advantageous for known study sites and years, while the inclusion of both optical and SAR data yields favorable results for transferable models. Additionally, weather data was found to play a significant role in classifying mowing events for known study sites and years. However, caution is necessary when incorporating weather data into transferable models, as it may reduce their performance on unknown sites or years.

For transferable models specifically applicable to CAP monitoring, this study suggests utilizing a CNN model with optical and SAR data, excluding weather data. But it is important to acknowledge that while the results partially support this approach, further research is necessary to obtain more conclusive findings in this regard.

In summary, our study provides valuable insights for researchers and practitioners in selecting appropriate methods and feature combinations tailored to their specific study requirements. By improving the accuracy and applicability of models in diverse contexts, these findings enhance the effectiveness of mowing event detection and contribute to advancements in related fields.

CRediT authorship contribution statement

Ann-Kathrin Holtgrave: Conceptualization, Methodology, Software, Validation, Formal analysis, Writing – original draft, Writing – review & editing, Visualization. **Felix Lobert:** Methodology, Software, Writing – review & editing. **Stefan Erasmi:** Conceptualization, Writing – review & editing. **Norbert Röder:** Conceptualization, Writing – review & editing. **Birgit Kleinschmit:** Conceptualization, Writing – review & editing.

Declaration of competing interest

The authors declare that they have no known competing financial interests or personal relationships that could have appeared to influence the work reported in this paper.

Data availability

The authors do not have permission to share data.

Acknowledgments

The authors would like to thank Kerstin Grant, Hansjörg Nußbaum, and Erwin Mohr (Landwirtschaftliches Zentrum für Rinderhaltung, Grünlandwirtschaft, Milchwirtschaft, Wild und Fischerei Baden-Württemberg (LAZBW)) for providing data of the experimental farm in Aulendorf. We gratefully give thanks to Hubert Kivelitz for supporting us with data from the experimental farm *Haus Riswick* of the North Rhine-Westphalia Chamber of Agriculture in Kleve, as well as Alexander Klein (Thuenen Institute, Institute of Organic Farming), head of the experimental farm in Trenthorst for providing valuable reference data. In addition, we are thankful for data from the Lindhof experimental farm of the Christian-Albrecht-University Kiel was provided by Christof Klußand Sabine Mues with the kind support of Prof. Dr. Taube, Department of Grass and Forage Science/ Organic Agriculture. We further thank the managers of the three Biodiversity Exploratories, Kirsten Reichel-Jung, Iris Steitz, Sandra Weithmann, Florian Staub, Juliane Vogt, Anna K. Franke, Miriam Teuscher and all former managers for their work in maintaining the plot and project infrastructure; Christiane Fischer and Victoria Grießmeier for giving support through the central office, Andreas Ostrowski for managing the central data base, and Markus Fischer, Eduard Linsenmair, Dominik Hessenmöller, Daniel Prati, Ingo Schöning, François Buscot, Ernst-Detlef Schulze, Wolfgang W. Weisser and the late Elisabeth Kalko for their role in setting up the Biodiversity Exploratories project. We thank the administration of the Hainich national park, the UNESCO Biosphere Reserve Swabian Alb and the UNESCO Biosphere Reserve Schorfheide-Chorin as well as all landowners for the excellent collaboration. The work has been (partly) funded by the DFG, Germany Priority Program 1374 "Biodiversity-Exploratories" (DFG-Refno.). Field work permits were issued by the responsible state environmental offices of Baden-Württemberg, Thüringen, and Brandenburg. All authors have read and agreed to the published version of the manuscript.

Appendix. Tables

See Tables A.6–A.9.

Table A.6
Transferability by Testsite: Classification metrics for mowing event classification by algorithm, gap handling and features. F1, Recall (TPR) and Precision (PPV) are shown. The list is ordered by descending F1.

Method	Gap-handling	Feature	Weather	F1	PPV	TPR
CNN	Gap-Filled	OPT	+ W	0.76	0.66	0.90
CNN	Gap-Filled	OPT+SAR	−W	0.74	0.62	0.91
CNN	Lin. interpolated	OPT+SAR	−W	0.73	0.65	0.84
CNN	Lin. interpolated	OPT	+ W	0.70	0.66	0.73
CNN	Gap-Filled	OPT	−W	0.69	0.63	0.77
LSTM	Gap-Filled	OPT+SAR	+ W	0.69	0.61	0.78
LSTM	Lin. interpolated	OPT+SAR	−W	0.69	0.60	0.82
CNN	Gap-Filled	OPT+SAR	+ W	0.68	0.61	0.78
LSTM	Gap-Filled	OPT+SAR	−W	0.68	0.60	0.79
SVM	Lin. interpolated	OPT+SAR	−W	0.68	0.53	0.93
SVM	Lin. interpolated	OPT	−W	0.68	0.56	0.85
CNN	Lin. interpolated	OPT+SAR	+ W	0.67	0.64	0.69
CNN	Lin. interpolated	OPT	−W	0.67	0.64	0.69
LSTM	Lin. interpolated	OPT+SAR	+ W	0.67	0.58	0.78
SVM	Gap-Filled	OPT+SAR	−W	0.65	0.49	0.96
SVM	Gap-Filled	OPT	−W	0.65	0.49	0.97
CNN		SAR	−W	0.62	0.54	0.72
LSTM	Gap-Filled	OPT	−W	0.62	0.54	0.72
LSTM	Gap-Filled	OPT	+ W	0.61	0.55	0.68
SVM	Lin. interpolated	OPT+SAR	+ W	0.61	0.49	0.81
LSTM	Lin. interpolated	OPT	−W	0.60	0.58	0.62
SVM	Gap-Filled	OPT+SAR	+ W	0.59	0.45	0.85
SVM	Gap-Filled	OPT	+ W	0.59	0.46	0.84
SVM	Lin. interpolated	OPT	+ W	0.59	0.46	0.81
LSTM	Lin. interpolated	OPT	+ W	0.58	0.61	0.55
LSTM		SAR	−W	0.55	0.48	0.65
SVM		SAR	−W	0.55	0.40	0.89
LSTM		SAR	+ W	0.52	0.49	0.55
SVM		SAR	+ W	0.51	0.37	0.81
RF	Gap-Filled	OPT	−W	0.45	0.81	0.31
CNN		SAR	+ W	0.30	0.35	0.26
RF	Lin. interpolated	OPT	−W	0.30	0.86	0.18
RF	Gap-Filled	OPT	+ W	0.27	0.88	0.16
RF	Lin. interpolated	OPT	+ W	0.21	0.82	0.12
RF	Gap-Filled	OPT+SAR	−W	0.12	0.83	0.06
RF	Lin. interpolated	OPT+SAR	−W	0.07	0.75	0.04
RF		SAR	−W	0.02	0.67	0.01
RF	Gap-Filled	OPT+SAR	+ W	NA	NA	0.00
RF		SAR	+ W	NA	NA	0.00
RF	Lin. interpolated	OPT+SAR	+ W	NA	NA	0.00

Table A.7
Transferability by Year, target 2017: Classification metrics for mowing event classification by algorithm, gap handling and features. F1, Recall (TPR) and Precision (PPV) are shown. The list is ordered by descending F1.

Method	Gap-handling	Feature	Weather	F1	PPV	TPR
CNN	Gap-Filled	OPT+SAR	−W	0.72	0.68	0.77
CNN	Gap-Filled	OPT	−W	0.72	0.62	0.84
CNN	Lin. interpolated	OPT+SAR	−W	0.72	0.68	0.77
CNN	Lin. interpolated	OPT+SAR	+ W	0.71	0.63	0.80
SVM	Gap-Filled	OPT	−W	0.70	0.58	0.89
CNN	Gap-Filled	OPT+SAR	+ W	0.69	0.65	0.73
CNN	Lin. interpolated	OPT	−W	0.69	0.62	0.78
SVM	Gap-Filled	OPT+SAR	−W	0.69	0.56	0.90
SVM	Lin. interpolated	OPT+SAR	−W	0.69	0.56	0.89
LSTM	Gap-Filled	OPT	−W	0.67	0.61	0.75
LSTM	Lin. interpolated	OPT+SAR	−W	0.67	0.66	0.68
CNN	Gap-Filled	OPT	+ W	0.66	0.64	0.68
LSTM	Gap-Filled	OPT+SAR	−W	0.66	0.65	0.67
SVM	Gap-Filled	OPT	+ W	0.64	0.52	0.86
SVM	Lin. interpolated	OPT	−W	0.64	0.53	0.81
LSTM	Lin. interpolated	OPT+SAR	+ W	0.63	0.66	0.60
CNN		SAR	+ W	0.62	0.58	0.67
CNN		SAR	−W	0.62	0.56	0.69
LSTM	Gap-Filled	OPT+SAR	+ W	0.61	0.59	0.62
CNN	Lin. interpolated	OPT	+ W	0.60	0.58	0.62
LSTM	Lin. interpolated	OPT	−W	0.60	0.63	0.57
SVM	Lin. interpolated	OPT	+ W	0.59	0.47	0.77
LSTM	Gap-Filled	OPT	+ W	0.55	0.60	0.51
LSTM	Gap-Filled	SAR	−W	0.54	0.56	0.53
LSTM	Lin. interpolated	OPT	+ W	0.54	0.61	0.49
SVM		SAR	+ W	0.54	0.42	0.77
LSTM		SAR	+ W	0.47	0.51	0.45
RF	Gap-Filled	OPT	−W	0.35	0.76	0.22
RF	Lin. interpolated	OPT	−W	0.29	0.87	0.18
RF	Lin. interpolated	OPT	+ W	0.08	0.81	0.04
RF	Gap-Filled	OPT+SAR	−W	0.05	0.79	0.03
RF	Gap-Filled	OPT	+ W	0.05	0.85	0.03
RF	Lin. interpolated	OPT+SAR	−W	0.02	0.80	0.01
RF		SAR	−W	0.00	1.00	0.00
RF	Gap-Filled	OPT+SAR	+ W	NA	NA	0.00
RF		SAR	+ W	NA	NA	0.00
RF	Lin. interpolated	OPT+SAR	+ W	NA	NA	0.00
SVM	Gap-Filled	OPT+SAR	+ W	NA	NA	0.00
SVM		SAR	−W	NA	NA	NA
SVM	Lin. interpolated	OPT+SAR	+ W	NA	NA	0.00

Table A.8
Transferability by Year, target 2018: Classification metrics for mowing event classification by algorithm, gap handling and features. F1, Recall (TPR) and Precision (PPV) are shown. The list is ordered by descending F1.

Method	Gap-handling	Feature	Weather	F1	PPV	TPR
CNN	Gap-Filled	OPT	−W	0.72	0.72	0.71
CNN	Gap-Filled	OPT+SAR	−W	0.71	0.82	0.62
SVM	Gap-Filled	OPT	−W	0.71	0.63	0.81
CNN	Lin. Interpolated	OPT+SAR	−W	0.70	0.76	0.64
CNN	Lin. Interpolated	OPT+SAR	+ W	0.68	0.80	0.59
SVM	Gap-Filled	OPT+SAR	−W	0.68	0.60	0.79
SVM	Lin. Interpolated	OPT	−W	0.66	0.56	0.79
SVM	Lin. Interpolated	OPT+SAR	−W	0.65	0.55	0.79
CNN	Lin. Interpolated	OPT	−W	0.64	0.59	0.70
LSTM	Gap-Filled	OPT	−W	0.64	0.68	0.60
CNN	Lin. Interpolated	OPT	+ W	0.63	0.81	0.52
LSTM	Lin. Interpolated	OPT	−W	0.63	0.65	0.61
CNN	Gap-Filled	OPT	+ W	0.61	0.77	0.50
LSTM	Gap-Filled	OPT+SAR	−W	0.61	0.69	0.56
LSTM	Lin. Interpolated	OPT+SAR	−W	0.61	0.66	0.56
CNN		SAR	−W	0.60	0.57	0.62
LSTM	Gap-Filled	OPT	+ W	0.60	0.74	0.50
SVM	Gap-Filled	OPT	+ W	0.60	0.57	0.64
SVM	Lin. Interpolated	OPT+SAR	+ W	0.60	0.58	0.62
CNN	Gap-Filled	OPT+SAR	+ W	0.59	0.88	0.44
SVM	Gap-Filled	OPT+SAR	+ W	0.59	0.57	0.61
CNN		SAR	+ W	0.58	0.65	0.52
LSTM	Lin. Interpolated	OPT+SAR	+ W	0.58	0.62	0.55

Table A.8 (*continued*).

Method	Gap-handling	Feature	Weather	F1	PPV	TPR
LSTM	Lin. Interpolated	OPT	+ W	0.54	0.67	0.45
SVM	Lin. Interpolated	OPT	+ W	0.54	0.47	0.65
LSTM	Gap-Filled	OPT+SAR	+ W	0.53	0.62	0.46
LSTM		SAR	+ W	0.49	0.56	0.44
LSTM		SAR	−W	0.41	0.44	0.38
RF	Gap-Filled	OPT	−W	0.38	0.90	0.24
RF	Lin. Interpolated	OPT	−W	0.26	0.9	0.15
RF	Lin. Interpolated	OPT	+ W	0.15	0.64	0.09
RF	Gap-Filled	OPT	+ W	0.10	1.00	0.05
RF	Gap-Filled	OPT+SAR	−W	0.06	1.00	0.03
RF	Lin. Interpolated	OPT+SAR	−W	0.05	1.00	0.02
RF	Gap-Filled	OPT+SAR	+ W	NA	NA	0.00
RF		SAR	+ W	NA	NA	0.00
RF		SAR	−W	NA	NA	0.00
RF	Lin. Interpolated	OPT+SAR	+ W	NA	NA	0.00
SVM		SAR	+ W	NA	NA	0.00
SVM		SAR	−W	NA	NA	NA

Table A.9
Transferability by Year, target 2019: Classification metrics for mowing event classification by algorithm, gap handling and features. F1, Recall (TPR) and Precision (PPV) are shown. The list is ordered by descending F1.

Method	Gap-handling	Feature	Weather	F1	PPV	TPR
CNN	Gap-Filled	OPT	−W	0.80	0.74	0.87
CNN	Gap-Filled	OPT+SAR	−W	0.79	0.76	0.82
LSTM	Gap-Filled	OPT+SAR	−W	0.77	0.79	0.75
CNN	Lin. interpolated	OPT+SAR	+ W	0.76	0.71	0.82
SVM	Gap-Filled	OPT	−W	0.76	0.66	0.90
CNN	Lin. interpolated	OPT+SAR	−W	0.75	0.67	0.85
CNN	Lin. interpolated	OPT	−W	0.75	0.70	0.81
CNN	Gap-Filled	OPT+SAR	+ W	0.74	0.79	0.70
SVM	Gap-Filled	OPT+SAR	−W	0.74	0.61	0.95
LSTM	Gap-Filled	OPT	−W	0.73	0.68	0.78
SVM	Lin. interpolated	OPT+SAR	−W	0.73	0.61	0.93
SVM	Lin. interpolated	OPT	−W	0.73	0.64	0.87
SVM	Gap-Filled	OPT	+ W	0.72	0.60	0.92
LSTM	Gap-Filled	OPT+SAR	+ W	0.71	0.78	0.65
LSTM	Lin. interpolated	OPT+SAR	−W	0.71	0.74	0.69
LSTM	Lin. interpolated	OPT+SAR	+ W	0.70	0.79	0.62
LSTM	Lin. interpolated	OPT	−W	0.69	0.71	0.67
CNN	Gap-Filled	OPT	+ W	0.68	0.75	0.62
LSTM	Gap-Filled	OPT	+ W	0.68	0.73	0.63
LSTM	Lin. interpolated	OPT	+ W	0.67	0.77	0.60
CNN	Lin. interpolated	OPT	+ W	0.66	0.71	0.61
SVM	Gap-Filled	OPT+SAR	+ W	0.66	0.53	0.87
SVM	Lin. interpolated	OPT	+ W	0.66	0.54	0.85
CNN		SAR	+ W	0.64	0.68	0.60
SVM	Lin. interpolated	OPT+SAR	+ W	0.63	0.5	0.84
SVM		SAR	−W	0.61	0.48	0.83
CNN		SAR	−W	0.55	0.50	0.60
SVM		SAR	+ W	0.55	0.42	0.79
LSTM		SAR	+ W	0.54	0.68	0.45
LSTM		SAR	−W	0.54	0.59	0.50
RF	Gap-Filled	OPT	−W	0.46	0.92	0.30
RF	Lin. interpolated	OPT	−W	0.45	0.97	0.30
RF	Gap-Filled	OPT	+ W	0.13	1.00	0.07
RF	Gap-Filled	OPT+SAR	−W	0.10	1.00	0.05
RF	Lin. interpolated	OPT+SAR	−W	0.05	1.00	0.02
RF	Lin. interpolated	OPT	+ W	0.02	0.8	0.01
RF	Gap-Filled	OPT+SAR	+ W	NA	NA	0.00
RF		SAR	+ W	NA	NA	0.00
RF		SAR	−W	NA	NA	0.00
RF	Lin. interpolated	OPT+SAR	+ W	NA	NA	0.00

References

Allaire, J., Cholle, F., 2021. Keras: R interface to 'keras': R package version 2.7.0.

Belda, S., Pipia, L., Morcillo-Pallarés, P., Rivera-Caicedo, J.P., Amin, E., de Grave, C., Verrelst, J., 2020. DATimeS: A machine learning time series GUI toolbox for gap-handling and vegetation phenology trends detection. Environ. Model. Softw. 127, 104666. http://dx.doi.org/10.1016/j.envsoft.2020.104666.

Belgiu, M., Drăgu, L., 2016. Random forest in remote sensing: A review of applications and future directions. ISPRS J. Photogramm. Remote Sens. 114 (Part A), 24–31.

http://dx.doi.org/10.1016/j.isprsjprs.2016.01.011.
Bermudez, J.D., Happ, P.N., Feitosa, R.Q., Oliveira, D.A.B., 2019. Synthesis of multispectral optical images from SAR/Optical multitemporal data using conditional generative adversarial networks. IEEE Geosci. Remote Sens. Lett. 16 (8), 1220–1224. http://dx.doi.org/10.1109/LGRS.2019.2894734.
Bisphop, C.M., 1995. Neural Networks for Pattern Recognition. Oxford University Press, USA.
Blickensdörfer, L., Schwieder, M., Pflugmacher, D., Nendel, C., Erasmi, S., Hostert, P., 2022. Mapping of crop types and crop sequences with combined time series of Sentinel-1, Sentinel-2 and landsat 8 data for Germany. Remote Sens. Environ. 269, 112831. http://dx.doi.org/10.1016/j.rse.2021.112831.
Bogner, C., Seo, B., Rohner, D., Reineking, B., 2018. Classification of rare land cover types: Distinguishing annual and perennial crops in an agricultural catchment in South Korea. PLoS One 13 (1), e0190476. http://dx.doi.org/10.1371/journal.pone.0190476.
Bolton, D.K., Gray, J.M., Melaas, E.K., Moon, M., Eklundh, L., Friedl, M.A., 2020. Continental-scale land surface phenology from harmonized Landsat 8 and Sentinel-2 imagery. Remote Sens. Environ. 240 (6), 111685. http://dx.doi.org/10.1016/j.rse.2020.111685.
Breiman, L., 2001. Random forests. Mach. Learn. 45 (1), 5–32. http://dx.doi.org/10.1023/A:1010933404324.
Brown, L.J., Nocera, J.J., 2017. Conservation of breeding grassland birds requires local management strategies when hay maturation and nutritional quality differ among regions. Agric. Ecosys. Environ. 237, 242–249. http://dx.doi.org/10.1016/j.agee.2016.11.004.
Buddeberg, M., Bach, H., Hodrius, M., Paulik, F., Migdall, S., Kuhn, G., 2016. Potentials and limitations of optical and radar satellite imagery for grassland monitoring. In: Ouwehand, L. (Ed.), Proceedings of Living Planet Symposium 2016. In: ESA SP, ESA Communications, Noordwijk, The Netherlands.
Bundesanstalt für Landwirtschaft und Ernährung, 2017. Agrarmeteorologie. Bonn.
Chawla, N.V., Bowyer, K.W., Hall, L.O., Kegelmeyer, W.P., 2002. SMOTE: Synthetic minority over-sampling technique. J. Artificial Intelligence Res. 16, 321–357. http://dx.doi.org/10.1613/jair.953.
Chen, Y., He, W., Yokoya, N., Huang, T.Z., 2019. Blind cloud and cloud shadow removal of multitemporal images based on total variation regularized low-rank sparsity decomposition. ISPRS J. Photogramm. Remote Sens. 157 (2), 93–107. http://dx.doi.org/10.1016/j.isprsjprs.2019.09.003.
Claverie, M., Ju, J., Masek, J.G., Dungan, J.L., Vermote, E.F., Roger, J.C., Skakun, S.V., Justice, C., 2018. The Harmonized Landsat and Sentinel-2 surface reflectance data set. Remote Sens. Environ. 219 (2), 145–161. http://dx.doi.org/10.1016/j.rse.2018.09.002.
Corbane, C., Lang, S., Pipkins, K., Alleaume, S., Deshayes, M., García Millán, V.E., Strasser, T., Vanden Borre, J., Toon, S., Michael, F., 2015. Remote sensing for mapping natural habitats and their conservation status – New opportunities and challenges. Int. J. Appl. Earth Obs. Geoinf. 37 (3), 7–16. http://dx.doi.org/10.1016/j.jag.2014.11.005.
Courault, D., Hadria, R., Ruget, F., Olioso, A., Duchemin, B., Hagolle, O., Dedieu, G., 2010. Combined use of FORMOSAT-2 images with a crop model for biomass and water monitoring of permanent grassland in Mediterranean region. Hydrol. Earth Syst. Sci. 14 (9), 1731–1744. http://dx.doi.org/10.5194/hess-14-1731-2010.
Cresson, R., Ienco, D., Gaetano, R., Ose, K., Tong Minh, D.H., 2019. Optical image gap handling using deep convolutional autoencoder from optical and radar images. In: IGARSS 2019 - 2019 IEEE International Geoscience and Remote Sensing Symposium. IEEE, pp. 218–221. http://dx.doi.org/10.1109/IGARSS.2019.8900353.
Dahiya, N., Gupta, S., Singh, S., 2022. A review paper on machine learning applications, advantages, and techniques. ECS Trans. 107 (1), 6137–6150. http://dx.doi.org/10.1149/10701.6137ecst.
de Carvalho, O.A., Guimaraes, R.F., Trancoso Gomes, R.A., da Silva, N.C., 2017. Time series interpolation. In: IEEE International Geoscience and Remote Sensing Symposium. IEEE, pp. 1959–1961. http://dx.doi.org/10.1109/IGARSS.2007.4423211.
de Vroey, M., de Vendictis, L., Zavagli, M., Bontemps, S., Heymans, D., Radoux, J., Koetz, B., Defourny, P., 2022. Mowing detection using Sentinel-1 and Sentinel-2 time series for large scale grassland monitoring. Remote Sens. Environ. 280, 113145. http://dx.doi.org/10.1016/j.rse.2022.113145.
de Vroey, M., Radoux, J., Defourny, P., 2021. Grassland mowing detection using Sentinel-1 time series: Potential and limitations. Remote Sens. 13 (3), 348. http://dx.doi.org/10.3390/rs13030348.
de Vroey, M., Radoux, J., Defourny, P., 2023. Classifying sub-parcel grassland management practices by optical and microwave remote sensing. Remote Sens. 15 (1), 181. http://dx.doi.org/10.3390/rs15010181.
Dierschke, H., Briemle, G., Kratochwil, A., 2002. Kulturgrasland: Wiesen, Weiden Und Verwandte Staudenfluren. In: Ökosysteme Mitteleuropas aus geobotanischer Sicht, Verlag Eugen Ulmer, Stuttgart.
Döhler, H., 2009. Faustzahlen für die Landwirtschaft, 14. Aufl. ed. KTBL, Darmstadt.
Dusseux, P., Gong, X., Hubert-Moy, L., Corpetti, T., 2014a. Identification of grassland management practices from leaf area index time series. J. Appl. Remote Sens. 8 (1), 083559. http://dx.doi.org/10.1117/1.JRS.8.083559.
Dusseux, P., Vertès, F., Corpetti, T., Corgne, S., Hubert-Moy, L., 2014b. Agricultural practices in grasslands detected by spatial remote sensing. Environ. Monit. Assess. 186 (12), 8249–8265. http://dx.doi.org/10.1007/s10661-014-4001-5.
DWD Climate Data Center, 2021a. Annual regional averages of air temperature (annual mean) in °C (2 mabove ground), version v19.3. Last accessed 10 May 2021.
DWD Climate Data Center, 2021b. Annual regional averages of sunshine duration (annual sum) in hours,version v19.3. Last accessed 10 May 2021.
DWD Climate Data Center, 2021c. DWD climate data center (CDC): Annual regional averages of precipitation height (annual sum) in mm,version v19.3. Last accessed 10 May 2021.
Ernst, p., Loeper, E.G., Temperaturentwicklung und Vegetationsbeginn auf dem Grünland. Das Wirtschaftseigene Futter (22), 5–12.
Estel, S., Mader, S., Levers, C., Verburg, P.H., Baumann, M., Kuemmerle, T., 2018. Combining satellite data and agricultural statistics to map grassland management intensity in europe. Environ. Res. Lett. 13 (7), 074020. http://dx.doi.org/10.1088/1748-9326/aacc7a.
European Commission, 2018. Modernising the CAP: Satellite Data Authorised to Replace On-Farm Checks. Brussels, Belgium, URL: https://ec.europa.eu/info/news/modernising-cap-satellite-data-authorised-replace-farm-checks-2018-may-25_en.
European Union, 2021a. Regulation (EU) 2021/2115 of the European Parliament and of the Council of 2 December 2021 establishing rules on support for strategic plans to be drawn up by Member States under the common agricultural policy (CAP Strategic Plans) and financed by the European Agricultural Guarantee Fund (EAGF) and by the European Agricultural Fund for Rural Development (EAFRD) and repealing Regulations (EU) No 1305/2013 and (EU) No 1307/2013: Regulation (EU) 2021/2115. Off. J. Eur. Union L 435 (64), 1–186.
European Union, 2021b. Regulation (EU) 2021/2116 of the European Parliament and of the Council of 2 December 2021 on the financing, management and monitoring of the common agricultural policy and repealing Regulation (EU) No 1306/2013: Regulation (EU) 2021/2116. Off. J. Eur. Union L 435 (64), 187–261.
Eurostat, 2018. Land cover overview by NUTS 2 regions.
Fabel, D., Allaire, J., RStudio, Tang, Y., Eddelbuettel, D., Golding, N., Kalinowski, T., Google Inc., 2022. tensorflow: R interface to 'TensorFlow'. URL: https://cran.r-project.org/web/packages/tensorflow/tensorflow.pdf.
Filipponi, F., 2019. Sentinel-1 GRD preprocessing workflow. Proceedings 18 (1), 11. http://dx.doi.org/10.3390/ECRS-3-06201.
Fischer, M., Bossdorf, O., Gockel, S., Hänsel, F., Hemp, A., Hessenmöller, D., Korte, G., Nieschulze, J., Pfeiffer, S., Prati, D., Renner, S., Schöning, I., Schumacher, U., Wells, K., Buscot, F., Kalko, E.K., Linsenmair, K.E., Schulze, E.D., Weisser, W.W., 2010. Implementing large-scale and long-term functional biodiversity research: The biodiversity exploratories. Basic Appl. Ecol. 11 (6), 473–485. http://dx.doi.org/10.1016/j.baae.2010.07.009.
Fischer, C., Tischer, J., Roscher, C., Eisenhauer, N., Ravenek, J., Gleixner, G., Attinger, S., Jensen, B., de Kroon, H., Mommer, L., Scheu, S., Hildebrandt, A., 2015. Plant species diversity affects infiltration capacity in an experimental grassland through changes in soil properties. Plant Soil 397 (1–2), 1–16. http://dx.doi.org/10.1007/s11104-014-2373-5.
Frantz, D., 2019. FORCE—Landsat + Sentinel-2 analysis ready data and beyond. Remote Sens. 11 (9), 1124. http://dx.doi.org/10.3390/rs11091124.
García-Feced, C., Weissteiner, C.J., Baraldi, A., Paracchini, M.L., Maes, J., Zulian, G., Kempen, M., Elbersen, B., Pérez-Soba, M., 2015. Semi-natural vegetation in agricultural land: European map and links to ecosystem service supply. Agron. Sustain. Dev. 35 (1), 273–283. http://dx.doi.org/10.1007/s13593-014-0238-1.
Garioud, A., Valero, S., Giordano, S., Mallet, C., 2020. On the joint exploitation of optical and SAR satellite imagery for grassland monitoring. ISPRS - Int. Arch. Photogramm. Remote Sens. Spatial Inf. Sci. XLIII-B3-2020, 591–598. http://dx.doi.org/10.5194/isprs-archives-XLIII-B3-2020-591-2020.
Garioud, A., Valero, S., Giordano, S., Mallet, C., 2021. Recurrent-based regression of sentinel time series for continuous vegetation monitoring. Remote Sens. Environ. 263, 112419. http://dx.doi.org/10.1016/j.rse.2021.112419.
German Weather Center, 2020. Climate data of the dwd; synop data from the time series 1960–2020; averaged from original single data.
Goodfellow, I., Bengio, Y., Courville, A., 2016. Deep Learning. MIT Press.
Grant, K., Siegmund, R., Wagner, M., Hartmann, S., 2015a. Satellite-based assessment of grassland yields. ISPRS - Int. Arch. Photogramm. Remote Sens. Spatial Inf. Sci. XL-7/W3, 15–18. http://dx.doi.org/10.5194/isprsarchives-XL-7-W3-15-2015.
Grant, K., Siegmund, R., Wagner, M., Kluß, C., Herrmann, A., Taube, F., Hartmann, S., 2015b. Regionalisierte Erfassung von Nutzungsintensitäten im Grünland mittels Radartechnik. In: Francke-Weltmann (Ed.), Multifunktionale Agrarlandschaften - Pflanzenbaulicher Anspruch, Biodiversität, Ökosystemdienstleistungen, Vol. 27. Verlag Liddy Halm Göttingen, Göttingen, pp. 113–114.
Griffiths, P., Nendel, C., Pickert, J., Hostert, P., 2019. Towards national-scale characterization of grassland use intensity from integrated Sentinel-2 and landsat time series. Remote Sens. Environ. 111124. http://dx.doi.org/10.1016/j.rse.2019.03.017.
Hajduch, G., Bourbigot, M., 2022. Sentinel-1 Product Specification. S1-RS-MDA-52-7441, European Space Agency.
Halabuk, A., Mojses, M., Halabuk, M., David, S., 2015. Towards detection of cutting in hay meadows by using of NDVI and EVI time series. Remote Sens. 7 (5), 6107–6132. http://dx.doi.org/10.3390/rs70506107.
Hinton, G.E., Salakhutdinov, R.R., 2006. Reducing the dimensionality of data with neural networks. Science 313 (5786), 504–507. http://dx.doi.org/10.1126/science.1127647.

Ho, T.K., 1995. Random decision forests. In: Proceedings of 3rd International Conference on Document Analysis and Recognition. IEEE Comput. Soc. Press, pp. 278–282. http://dx.doi.org/10.1109/ICDAR.1995.598994.

Hochreiter, S., Schmidhuber, J., 1997. Long short-term memory. Neural Comput. 9 (8), 1735–1780. http://dx.doi.org/10.1162/neco.1997.9.8.1735.

Holtgrave, A., Ackermann, A., Röder, N., Kleinschmit, B., 2020a. Towards a dual-polarisation radar vegetation index for Sentinel-1 for grassland monitoring. In: Meeting the Future Demands for Grassland Production. pp. 596–598.

Holtgrave, A.K., Röder, N., Ackermann, A., Erasmi, S., Kleinschmit, B., 2020b. Comparing Sentinel-1 and -2 data and indices for agricultural land use monitoring. Remote Sens. 12 (18), 2919. http://dx.doi.org/10.3390/rs12182919.

Huete, A., Didan, K., Miura, T., Rodriguez, E., Gao, X., Ferreira, L., 2002. Overview of the radiometric and biophysical performance of the MODIS vegetation indices. Remote Sens. Environ. 83 (1–2), 195–213. http://dx.doi.org/10.1016/S0034-4257(02)00096-2.

Jankowska-Huflejt, H., 2006. The function of permanent grasslands in water resources protection. J. Water Land Dev. 10 (1), http://dx.doi.org/10.2478/v10025-007-0005-7.

Jin, X., Tang, P., Houet, T., Corpetti, T., Alvarez-Vanhard, E.G., Zhang, Z., 2021. Sequence image interpolation via separable convolution network. Remote Sens. 13 (2), 296. http://dx.doi.org/10.3390/rs13020296.

Julien, Y., Sobrino, J.A., 2019. Optimizing and comparing gap-handling techniques using simulated NDVI time series from remotely sensed global data. Int. J. Appl. Earth Obs. Geoinf. 76 (7), 93–111. http://dx.doi.org/10.1016/j.jag.2018.11.008.

Kalinowski, T., Fabel, D., Allaire, J., Chollet, F., RStudio, Google Inc., Tang, Y., van der Bijl, W., Studer, M., Keydana, S., 2023. R interface to 'Keras'.

Kandasamy, S., Baret, F., Verger, A., Neveux, P., Weiss, M., 2013. A comparison of methods for smoothing and gap handling time series of remote sensing observations – application to MODIS LAI products. Biogeosciences 10 (6), 4055–4071. http://dx.doi.org/10.5194/bg-10-4055-2013.

Karim, F., Majumdar, S., Darabi, H., Harford, S., 2019. Multivariate LSTM-FCNs for time series classification. Neural Netw. Off. J. Int. Neural Netw. Soc. 116, 237–245. http://dx.doi.org/10.1016/j.neunet.2019.04.014.

Kent, A., Berry, M.M., Luehrs, F.U., Perry, J.W., 1955. Machine literature searching VIII. Operational criteria for designing information retrieval systems. Am. Doc. 6 (2), 93–101. http://dx.doi.org/10.1002/asi.5090060209.

Ketzer, D., Rösch, C., Haase, M., 2017. Assessment of sustainable grassland biomass potentials for energy supply in Northwest Europe. Biomass Bioenergy 100, 39–51. http://dx.doi.org/10.1016/j.biombioe.2017.03.009.

Kleijn, D., Kohler, F., Baldi, A., Batary, P., Concepcion, E., Clough, Y., Diaz, M., Gabriel, D., Holzschuh, A., Knop, E., Kovacs, A., Marshall, E., Tscharntke, T., Verhulst, J., 2009. On the relationship between farmland biodiversity and land-use intensity in Europe. Proc. R. Soc. Lond. [Biol.] 276 (1658), 903–909. http://dx.doi.org/10.1098/rspb.2008.1509.

Klimek, S., Richter gen. Kemmermann, A., Hofmann, M., Isselstein, J., 2007. Plant species richness and composition in managed grasslands: The relative importance of field management and environmental factors. Biol. Cons. 134 (4), 559–570. http://dx.doi.org/10.1016/j.biocon.2006.09.007.

Kolecka, N., Ginzler, C., Pazur, R., Price, B., Verburg, P., 2018. Regional scale mapping of grassland mowing frequency with Sentinel-2 time series. Remote Sens. 10 (8), 1221. http://dx.doi.org/10.3390/rs10081221.

Kuhn, M., Wing, J., Weston, S., Williams, A., Keefer, C., Engelhardt, A., Cooper, T., Mayer, Z., Kenkel, B., R Core Team, Benesty, M., Lescarbeau, R., Ziem, A., Scrucca, L., Tang, Y., Candan, C., Hunt, T., 2021. caret: Classification and regression training: Version 6.0-86. URL: https://CRAN.R-project.org/package=caret.

Li, J., Huang, X., Gong, J., 2019. Deep neural network for remote-sensing image interpretation: status and perspectives. Natl. Sci. Rev. 6 (6), 1082–1086. http://dx.doi.org/10.1093/nsr/nwz058.

Li, Z.L., Leng, P., Zhou, C., Chen, K.S., Zhou, F.C., Shang, G.F., 2021. Soil moisture retrieval from remote sensing measurements: Current knowledge and directions for the future. Earth-Sci. Rev. 218, 103673. http://dx.doi.org/10.1016/j.earscirev.2021.103673.

Li, M., Zang, S., Zhang, B., Li, S., Wu, C., 2014. A review of remote sensing image classification techniques: the role of spatio-contextual information. Eur. J. Remote Sen. 47 (1), 389–411. http://dx.doi.org/10.5721/EuJRS20144723.

Liakos, K.G., Busato, P., Moshou, D., Pearson, S., Bochtis, D., 2018. Machine learning in agriculture: A review. Sensors (Basel, Switzerland) 18 (8), http://dx.doi.org/10.3390/s18082674.

Ling, C.X., Li, C., 1998. Data mining for direct marketing: problems and solutions. In: Agrawal, R. (Ed.), Proceedings / the Fourth International Conference on Knowledge Discovery and Data Mining. AAAI Press, Menlo Park, Calif., pp. 73–79.

Lobert, F., Holtgrave, A.K., Schwieder, M., Pause, M., Vogt, J., Gocht, A., Erasmi, S., 2021. Mowing event detection in permanent grasslands: Systematic evaluation of input features from Sentinel-1, Sentinel-2, and Landsat 8 time series. Remote Sens. Environ. 267 (309), 112751. http://dx.doi.org/10.1016/j.rse.2021.112751.

Lu, J., Tan, L., Jiang, H., 2021. Review on convolutional neural network (CNN) applied to plant leaf disease classification. Agriculture 11 (8), 707. http://dx.doi.org/10.3390/agriculture11080707.

Mazza, A., Gargiulo, M., Scarpa, G., Gaetano, R., 2018. Estimating the NDVI from SAR by convolutional neural networks. In: IGARSS 2018 - 2018 IEEE International Geoscience and Remote Sensing Symposium. pp. 1954–1957. http://dx.doi.org/10.1109/IGARSS.2018.8519459.

McIntosh, D.W., Bates, G.E., Keyser, P.D., Allen, F.L., Harper, C.A., Waller, J.C., Birckhead, J.L., Backus, W.M., 2016. Forage harvest timing impact on biomass quality from native warm-season grass mixtures. Agron. J. 108 (4), 1524–1530. http://dx.doi.org/10.2134/agronj2015.0560.

Mitsch, W.J., Gosselink, J.G., 2000. The value of wetlands: Importance of scale and landscape setting. Ecol. Econom. 35 (1), 25–33. http://dx.doi.org/10.1016/S0921-8009(00)00165-8.

Moreno-Martínez, Á., Izquierdo-Verdiguier, E., Maneta, M.P., Camps-Valls, G., Robinson, N., Muñoz-Marí, J., Sedano, F., Clinton, N., Running, S.W., 2020. Multispectral high resolution sensor fusion for smoothing and gap-handling in the cloud. Remote Sens. Environ. 247, 111901. http://dx.doi.org/10.1016/j.rse.2020.111901.

Mountrakis, G., Im, J., Ogole, C., 2011. Support vector machines in remote sensing: A review. ISPRS J. Photogramm. Remote Sens. 66 (3), 247–259. http://dx.doi.org/10.1016/j.isprsjprs.2010.11.001.

Nasirzadehdizaji, R., Balik Sanli, F., Abdikan, S., Cakir, Z., Sekertekin, A., Ustuner, M., 2019. Sensitivity analysis of multi-temporal Sentinel-1 SAR parameters to crop height and canopy coverage. Appl. Sci. 9 (4), 655. http://dx.doi.org/10.3390/app9040655.

O'Shea, K., Nash, R., 2015. An introduction to convolutional neural networks. http://dx.doi.org/10.48550/arXiv.1511.08458.

Peeters, A., 2009. Importance, evolution, environmental impact and future challenges of grasslands and grassland-based systems in europe. Grassland Sci. 55 (3), 113–125. http://dx.doi.org/10.1111/j.1744-697X.2009.00154.x.

Reinermann, S., Asam, S., Kuenzer, C., 2020. Remote sensing of grassland production and management—A review. Remote Sens. 12 (12), 1949. http://dx.doi.org/10.3390/rs12121949.

Reinermann, S., Gessner, U., Asam, S., Ullmann, T., Schucknecht, A., Kuenzer, C., 2022. Detection of grassland mowing events for Germany by combining Sentinel-1 and Sentinel-2 time series. Remote Sens. 14 (7), 1647. http://dx.doi.org/10.3390/rs14071647.

Richtlinie KULAP, 2020. Richtlinie des Ministeriums für Landwirtschaft, Umwelt und Klimaschutz des Landes Brandenburg zur Förderung umweltgerechter landwirtschaftlicher Produktionsverfahren und zur Erhaltung der Kulturlandschaft der Länder Brandenburg und Berlin (KULAP 2014) - II D 2.

Richtlinie NiB-AUM, 2019. Richtlinie über die Gewährung von Zuwendungen für Niedersächsischeund Bremer Agrarumweltmaßnahmen -NiB-AUM- (Fassung 15.3.2019) Gem.RdErl. d. MLu. d. MUv.15.7.2015 - GL 2.

Rieder, J., 1997. Extensive Bewirtschaftung von Dauergrünland. In: AID, vol. 1287, AID, Bonn.

Rosen, P.A., Hensley, S., Joughin, I.R., Li, F.K., Madsen, S.N., Rodriguez, E., Goldstein, R.M., 2000. Synthetic aperture radar interferometry. Proc. IEEE 88 (3), 333–382. http://dx.doi.org/10.1109/5.838084.

Rouse, J.W., Haas, R.H., Schell, J.A., Deering, D.W., 1973. Monitoring the Vernal Advancement and Retrogradation (Green Wave Effect) of Natural Vegetation. Progress Report RSC 1978-1, Texas, USA.

Scarpa, G., Gargiulo, M., Mazza, A., Gaetano, R., 2018. A CNN-based fusion method for feature extraction from sentinel data. Remote Sens. 10 (2), 236. http://dx.doi.org/10.3390/rs10020236.

Schlund, M., Erasmi, S., 2020. Sentinel-1 time series data for monitoring the phenology of winter wheat. Remote Sens. Environ. 246 (22), 111814. http://dx.doi.org/10.1016/j.rse.2020.111814.

Schmidt, T., Schuster, C., Kleinschmit, B., Forster, M., 2014. Evaluating an intra-annual time series for grassland classification—How many acquisitions and what seasonal origin are optimal? IEEE J. Sel. Top. Appl. Earth Obs. Remote Sens. 7 (8), 3428–3439. http://dx.doi.org/10.1109/JSTARS.2014.2347203.

Schmitt, M., Hughes, L.H., Zhu, X.X., 2018. The sen1-2 dataset for deep learning in sar-optical data fusion. ISPRS Ann. Photogramm. Remote Sens. Spatial Inf. Sci. IV-1, 141–146. http://dx.doi.org/10.5194/isprs-annals-IV-1-141-2018.

Schoof, N., Luick, R., Beaufoy, G., Jones, G., Einarsson, P., Ruiz, J., Stefanova, V., Fuchs, D., Windmaißer, T., Hötker, H., Jeromin, H., Nickel, H., Schumacher, J., Ukhanova, M. (Eds.), 2020. Grünlandschutz in Deutschland: Treiber der Biodiversität, Einfluss von Agrarumwelt- und Klimamaßnahmen, Ordnungsrecht, Molkereiwirtschaft und Auswirkungen der Klima- und Energiepolitik : Ergebnisse des F+E-Vorhabens "Auswirkungen der neuen Rahmenbedingungen der Gemeinsamen Agrarpolitik auf die Grünland-bezogene Biodiversität" (FKZ 3515 88 0100), 2. Auflage ed. In: BfN-Skripten, vol. 539, Bundesamt für Naturschutz, Bonn - Bad Godesberg.

Schuster, C., Ali, I., Lohmann, P., Frick, A., Förster, M., Kleinschmit, B., 2011. Towards detecting swath events in TerraSAR-X time series to establish NATURA 2000 grassland habitat swath management as monitoring parameter. Remote Sens. 3 (12), 1308–1322. http://dx.doi.org/10.3390/rs3071308.

Schwieder, M., Wesemeyer, M., Frantz, D., Pfoch, K., Erasmi, S., Pickert, J., Nendel, C., Hostert, P., 2022. Mapping grassland mowing events across Germany based on combined Sentinel-2 and Landsat 8 time series. Remote Sens. Environ. 269, 112795. http://dx.doi.org/10.1016/j.rse.2021.112795.

Sheykhmousa, M., Mahdianpari, M., Ghanbari, H., Mohammadimanesh, F., Ghamisi, P., Homayouni, S., 2020. Support vector machine versus random forest for remote sensing image classification: A meta-analysis and systematic review. IEEE J. Sel. Top. Appl. Earth Obs. Remote Sens. 13, 6308–6325. http://dx.doi.org/10.1109/JSTARS.2020.3026724.

Siegmund, R., Grant, K., Wagner, M., Hartmann, S., 2016. Satellite-based monitoring of grassland: assessment of harvest dates and frequency using SAR. In: Neale, C.M.U., Maltese, A. (Eds.), Remote Sensing for Agriculture, Ecosystems, and Hydrology XVIII. In: SPIE Proceedings, SPIE, 999803. http://dx.doi.org/10.1117/12.2240947.

Smit, H.J., Metzger, M.J., Ewert, F., 2008. Spatial distribution of grassland productivity and land use in europe. Agricult. Sys. 98 (3), 208–219. http://dx.doi.org/10.1016/j.agsy.2008.07.004.

Smith, R.S., Shiel, R.S., Millward, D., Corkhill, P., 2000. The interactive effects of management on the productivity and plant community structure of an upland meadow: an 8-year field trial. J. Appl. Ecol. 37 (6), 1029–1043. http://dx.doi.org/10.1046/j.1365-2664.2000.00566.x.

Socher, S.A., Prati, D., Boch, S., Müller, J., Klaus, V.H., Hölzel, N., Fischer, M., Wilson, S., 2012. Direct and productivity-mediated indirect effects of fertilization, mowing and grazing on grassland species richness. J. Ecol. 100 (6), 1391–1399. http://dx.doi.org/10.1111/j.1365-2745.2012.02020.x.

Soussana, J.F., Loiseau, P., Vuichard, N., Ceschia, E., Balesdent, J., Chevallier, T., Arrouays, D., 2004. Carbon cycling and sequestration opportunities in temperate grasslands. Soil Use Manag. 20 (2), 219–230. http://dx.doi.org/10.1111/j.1475-2743.2004.tb00362.x.

Statistisches Bundesamt, 2019. Land- und Forstwirtschaft, Fischerei: Bodennutzung der Betriebe (Landwirtschaftlich genutzte Flächen) 2019. Fachserie 3 Reihe 3.1.2.

Stendardi, L., Karlsen, S., Niedrist, G., Gerdol, R., Zebisch, M., Rossi, M., Notarnicola, C., 2019. Exploiting time series of Sentinel-1 and Sentinel-2 imagery to detect meadow phenology in mountain regions. Remote Sens. 11 (5), 542. http://dx.doi.org/10.3390/rs11050542.

Tamm, T., Zalite, K., Voormansik, K., Talgre, L., 2016. Relating Sentinel-1 interferometric coherence to mowing events on grasslands. Remote Sens. 8 (10), 802. http://dx.doi.org/10.3390/rs8100802.

Taravat, A., Wagner, M., Oppelt, N., 2019. Automatic grassland cutting status detection in the context of spatiotemporal Sentinel-1 imagery analysis and artificial neural networks. Remote Sens. 11 (6), 711. http://dx.doi.org/10.3390/rs11060711.

Thales Alenia Space Team, 2022. Sentinel-2 Product Specification: S2-PDGS-TAS-DI-PSD. URL: https://sentinel.esa.int/documents/247904/685211/S2-PDGS-TAS-DI-PSD-V14.9.pdf.

United States Geological Survey, 2019. Landsat 8 (L8): Data users handbook.

Vapnik, V.N., 2000. The Nature of Statistical Learning Theory, second ed. In: Statistics for Engineering and Information Science, Springer, New York, NY, URL: https://ebookcentral.proquest.com/lib/kxp/detail.action?docID=3086234.

Vogt, J., Klaus, V.H., Both, S., Fürstenau, C., Gockel, S., Gossner, M.M., Heinze, J., Hemp, A., Hölzel, N., Jung, K., Kleinebecker, T., Lauterbach, R., Lorenzen, K., Ostrowski, A., Otto, N., Prati, D., Renner, S., Schumacher, U., Seibold, S., Simons, N., Steitz, I., Teuscher, M., Thiele, J., Weithmann, S., Wells, K., Wiesner, K., Ayasse, M., Blüthgen, N., Fischer, M., Weisser, W.W., 2019. Eleven years' data of grassland management in Germany. Biodivers. Data J. 7, e36387. http://dx.doi.org/10.3897/bdj.7.e36387.

Voormansik, K., Jagdhuber, T., Olesk, A., Hajnsek, I., Papathanassiou, K.P., 2013. Towards a detection of grassland cutting practices with dual polarimetric TerraSAR-X data. Int. J. Remote Sens. 34 (22), 8081–8103. http://dx.doi.org/10.1080/01431161.2013.829593.

Voormansik, K., Zalite, K., Sünter, I., Tamm, T., Koppel, K., Verro, T., Brauns, A., Jakovels, D., Praks, J., 2020. Separability of mowing and ploughing events on short temporal baseline Sentinel-1 coherence time series. Remote Sens. 12 (22), 3784. http://dx.doi.org/10.3390/rs12223784.

Vreugdenhil, M., Wagner, W., Bauer-Marschallinger, B., Pfeil, I., Teubner, I., Rüdiger, C., Strauss, P., 2018. Sensitivity of sentinel-1 backscatter to vegetation dynamics: An Austrian case study. Remote Sens. 10 (9), 1396. http://dx.doi.org/10.3390/rs10091396.

Wang, J., Xiao, X., Bajgain, R., Starks, P., Steiner, J., Doughty, R.B., Chang, Q., 2019a. Estimating leaf area index and aboveground biomass of grazing pastures using Sentinel-1, Sentinel-2 and Landsat images. ISPRS J. Photogramm. Remote Sens. 154, 189–201. http://dx.doi.org/10.1016/j.isprsjprs.2019.06.007.

Wang, L., Xu, X., Yu, Y., Yang, R., Gui, R., Xu, Z., Pu, F., 2019b. SAR-to-optical image translation using supervised cycle-consistent adversarial networks. IEEE Access 7, 129136–129149. http://dx.doi.org/10.1109/ACCESS.2019.2939649.

Wang, Z., Yan, W., Oates, T., 2017. Time series classification from scratch with deep neural networks: A strong baseline. In: 2017 International Joint Conference on Neural Networks. IJCNN, IEEE, pp. 1578–1585. http://dx.doi.org/10.1109/IJCNN.2017.7966039.

Waramit, N., Moore, K.J., Fales, S.L., 2012. Forage quality of native warm-season grasses in response to nitrogen fertilization and harvest date. Anim. Feed Sci. Technol. 174 (1–2), 46–59. http://dx.doi.org/10.1016/j.anifeedsci.2012.02.008.

Weiner, C.N., Werner, M., Linsenmair, K.E., Blüthgen, N., 2011. Land use intensity in grasslands: Changes in biodiversity, species composition and specialisation in flower visitor networks. Basic Appl. Ecol. 12 (4), 292–299. http://dx.doi.org/10.1016/j.baae.2010.08.006.

Wrage, N., Strodthoff, J., Cuchillo, H.M., Isselstein, J., Kayser, M., 2011. Phytodiversity of temperate permanent grasslands: Ecosystem services for agriculture and livestock management for diversity conservation. Biodivers. Conserv. 20 (14), 3317–3339. http://dx.doi.org/10.1007/s10531-011-0145-6.

Zalite, K., Antropov, O., Praks, J., Voormansik, K., Noorma, M., 2016. Monitoring of agricultural grasslands with time series of X-Band repeat-pass interferometric SAR. IEEE J. Sel. Top. Appl. Earth Obs. Remote Sens. 9 (8), 3687–3697. http://dx.doi.org/10.1109/JSTARS.2015.2478120.

Zalite, K., Voormansik, K., Praks, J., Antropov, O., Noorma, M., 2014. Towards detecting mowing of agricultural grasslands from multi-temporal COSMO-SkyMed data. In: 2014 IEEE International Geoscience & Remote Sensing Symposium. IEEE, Piscataway, NJ, pp. 5076–5079. http://dx.doi.org/10.1109/IGARSS.2014.6947638.

Zhang, W., Tang, P., Zhao, L., 2019. Remote sensing image scene classification using CNN-CapsNet. Remote Sens. 11 (5), 494. http://dx.doi.org/10.3390/rs11050494.

Zhao, B., Lu, H., Chen, S., Liu, J., Wu, D., 2017. Convolutional neural networks for time series classification. J. Syst. Eng. Electron. 28 (1), 162–169. http://dx.doi.org/10.21629/JSEE.2017.01.18.

Zhao, W., Qu, Y., Chen, J., Yuan, Z., 2020. Deeply synergistic optical and SAR time series for crop dynamic monitoring. Remote Sens. Environ. 247, 111952. http://dx.doi.org/10.1016/j.rse.2020.111952.

Zou, J., Han, Y., So, S.S., 2008. Overview of artificial neural networks. Methods Mol. Biol. (Clifton, N.J.) 458, 15–23. http://dx.doi.org/10.1007/978-1-60327-101-1_2.